

DESIGN OF A TEMPERATURE PROGRAMMED DESORPTION SYSTEM FOR
THE MEASUREMENT OF THE DESORPTION KINETICS OF
MOLECULES FROM SURFACES

THESIS

Presented to the Graduate Council of
Texas State University-San Marcos
in Partial Fulfillment
of the Requirements

for the Degree

Master of SCIENCE

by

Nicholas J. Clark, B.S.

San Marcos, Texas
May 2009

DESIGN OF A TEMPERATURE PROGRAMMED DESORPTION SYSTEM FOR
THE MEASUREMENT OF THE DESORPTION KINETICS OF
MOLECULES FROM SURFACES

Committee Members Approved:

Carl A. Ventrice, Jr., Chair

Gregory F. Spencer

Heike Geisler

Approved:

J. Michael Willoughby
Dean of the Graduate College

COPYRIGHT

by

Nicholas J. Clark

2009

ACKNOWLEDGEMENTS

First and foremost I would like to thank God for bestowing many gifts upon me and surrounding me with so many noble and influential people my entire life. I would like to thank my father and mother for instilling in me the determination to excel in every endeavor while maintaining a humble spirit along the way. I know you don't hear me say it much because I rarely come home or call, but I love you and fully realize I would not have accomplished the achievements I have thus far without your love and support. To my sister and brother, April and Marcus, thank you for all of the "classic entertainment" that keeps me going when my brain is wore out from thinking about physics. You have no idea how much that helps. Thank you to the whole clan of Clarks, Bowers, and Borroughs, because as we all know, it truly "takes a village". To "tha brothahood", my football teammates, my musician friends, Edward, Mica, KC, and "lil t-dub" thank you for always providing the much needed break from physics and keeping me sane.

To my advisor, Carl, you are one of the most hard-working and knowledgeable people I know and I would like to thank you for all of your advice and direction. You have really helped me develop a love and interest for obtaining knowledge, not just about physics, but about any project that I am taking on.

This document was submitted April 15, 2009.

TABLE OF CONTENTS

	Page
ACKNOWLEDGEMENTS.....	iv
LIST OF FIGURES	vii
LIST OF TABLES.....	ix
ABSTRACT	x
CHAPTER	
I. INTRODUCTION.....	1
II. THEORY OF TPD.....	6
III. EXPERIMENTAL INSTRUMENTATION.....	11
A. Quadrupole Mass Spectrometer.....	11
B. Load Lock Chamber.....	14
C. Sample Holder and Stage.....	15
D. TPD IU	17
IV. EXPERIMENTAL CONTROL AND AUTOMATION.....	19
A. LabVIEW.....	19
B. MASsoft Professional.....	20
C. LabVIEW-TPD 8-mass measure.vi.....	22
D. LabVIEW-TPD RAMP.vi	31
V. RESULTS.....	39
A. Sample Preparation for Measurement.....	39
B. Pressure Program Preparation.....	41
C. Temperature Ramp Program Preparation.....	42
D. Analysis of TPD Spectra	47
1. $R_h \sim 50^\circ\text{C}/\text{min}$	47
2. $R_h \sim 25^\circ\text{C}/\text{min}$	48
3. $R_h \sim 10^\circ\text{C}/\text{min}$	49

E. Desorption Kinetics and Relative Coverages.....	50
F. Activation Energies.....	53
VI. DISCUSSION	57
VII. CONCLUSION	61
APPENDIX A: BLOCK DIAGRAMS.....	62
Partial Pressure Measurement Program.....	62
Temperature Ramp Program.....	63
APPENDIX B: CRACKING PATTERNS	64
REFERENCES	66

LIST OF FIGURES

Figure	Page
1. Graphene Oxide	4
2. Schematic of RGA probe.....	12
3. (a)Quadrupole Mass Spectrometer and (b)Interface Unit	13
4. Main Chamber and Load Lock Chamber	14
5. Sample Holder Stage and Thermocouple	15
6. Pin In/Out of DAQ Board.....	18
7. First Execution of Pressure Measurement Block Diagram	22
8. Measurement Parameters.....	25
9. First Execution Inside While Loop of Pressure Measurement	27
10. Data Formatting	29
11. Last Execution of Pressure Measurement Loop	30
12. First Execution of Temperature Ramp	31
13. Comparison Conditions	32
14. First Sequences in True Case Structure.....	33
15. Fourth Sequence in True Case Structure	34
16. Final Sequences of False Case Structure.....	36
17. Last Execution of Temperature Program.....	38
18. Optical Image of Films.....	40
19. Ramp with Linear Current Increase	43

20. Ramp with Varied Parameters-1	44
21. Ramp with Varied Parameters-2	45
22. Linear Temperature Ramp	45
23. Partial Pressure vs. Temperature Curves for $R_h \sim 50^\circ\text{C}/\text{min}$	47
24. Partial Pressure vs. Temperature Curves for $R_h \sim 25^\circ\text{C}/\text{min}$	48
25. Partial Pressure vs. Temperature Curves for $R_h \sim 10^\circ\text{C}/\text{min}$	49
26. CO_2 Partial Pressure vs. Temperature Curves	50
27. Activation Energies of CO_2	54
28. Ammonia Peaks	55

LIST OF TABLES

Table	Page
1. Polynomial Coefficients for K-type Thermocouple.....	16
2. Autorange Values of Each Respective Mass	41
3. Area Under Partial Pressure vs. Time Curves	51
4. Data for Slow-Stirred Films.....	53
5. Data for Ultrasonicated Films.....	53

ABSTRACT

DESIGN OF A TEMPERATURE PROGRAMMED DESORPTION SYSTEM FOR THE MEASUREMENT OF THE DESORPTION KINETICS OF MOLECULES FROM SURFACES

by

Nicholas J. Clark, B.S.

Texas State University-San Marcos

May 2009

SUPERVISING PROFESSOR: CARL A. VENTRICE JR.

Temperature programmed desorption (TPD) is an experimental technique used to measure the desorption kinetics of molecules from surfaces. This technique is performed by linearly increasing the temperature of a sample while measuring the partial pressures of the desorbing gas species. It is used to determine the relative coverage and activation energies of the desorbing species. To perform these measurements, a computer controlled feedback control system was designed that generates linear temperature ramps. In addition, a program was written to simultaneously measure up to eight partial pressures during the temperature ramp for the TPD measurements. This TPD system was used to examine the thermal stability of graphene oxide films and to determine the reduction kinetics of graphene oxide.

CHAPTER I

INTRODUCTION

Temperature programmed desorption (TPD) is a powerful analysis technique used to study the desorption of gases from the surfaces of materials in vacuum. The process involves a linear increase in the surface temperature of a sample while simultaneously observing the partial pressures of the desorbing molecules. Upon contact with a surface, species adsorb onto the surface either by physisorption, chemisorption, or by the formation of chemical bonds, minimizing the energy of the species. By increasing the surface temperature, energy is transferred to the system, and the species will eventually be given enough energy to desorb from the surface[4].

TPD gives information about the energy it takes for each respective molecule to desorb and the relative coverage of the desorbing molecules. The measurement of the partial pressures of the desorbing molecules is done with a mass spectrometer, which senses the mass to charge ratio (m/z) of the molecule. For the measurements done in this research project a quadrupole mass spectrometer was used. Since TPD is sensitive to the mass of the molecule, the process gives direct information about what is desorbing from the surface. In addition, TPD gives information about lateral interactions between adsorbates on the surface, which is known as the kinetics of desorption. This is done by giving a quantitative measure of the dependence on coverage of the desorption energy.

TPD has been used to obtain the kinetics of desorption and activation energies in chemical reduction studies of many important materials used for nanoscale technology.

Recent studies have shown that graphene is a potential candidate for use in nanoscale devices. Graphene is a flat monolayer of carbon atoms tightly packed into a two-dimensional honeycomb lattice structure, in essence, a single layer of graphite[11]. Graphene has received so much attention lately because of the exceptional electrical properties that result from its 2D nature[1]. Charge carriers can be tuned continuously between electrons and holes in concentrations as high as 10^{13} cm^{-2} and their mobilities can exceed $15,000 \text{ cm}^2\text{V}^{-1}\text{s}^{-1}$ even under ambient conditions[1]. These properties make it an ideal material for the production of integrated circuit components with nanoscale dimensions. In order to use graphene in integrated circuits, there exists a need for an inexpensive, scalable method for producing single-layer graphene on semiconducting or insulating surfaces.

Studies show that researchers have tried to make large scale graphene using the reduction of SiC to form a single carbon layer through the chemical depletion of Si[8]. This method of obtaining graphene, in which temperatures up to 1100°C are needed, results in uniformity and size domain issues of the films and in addition, proves to be very expensive. Another popular method is to prepare graphene using methane-based chemical vapor deposition on nickel films deposited over complete Si/SiO₂ wafers[9]. While single- and few-layer graphene were obtained, as confirmed by micro-Raman spectroscopy, problems occurred in making the layers well ordered. The method of thermally reducing single layer graphene oxide down to graphene is studied in this experiment.

Studies show that graphite oxide is easily exfoliated into single layer graphene oxide. Graphite oxide is formed through chemical oxidation of graphite and is known as the *Hummer's method*[10]. Graphite oxide is a multi-layer material consisting of graphene-derived sheets which have hydroxyl, epoxide and monoxide groups on their basal planes, and carbonyl and carboxyl groups situated at the edges. These graphene-derived sheets are called graphene oxide sheets. The actual structure of graphene oxide is not known but proposed theoretical models are shown below in Figure 1.

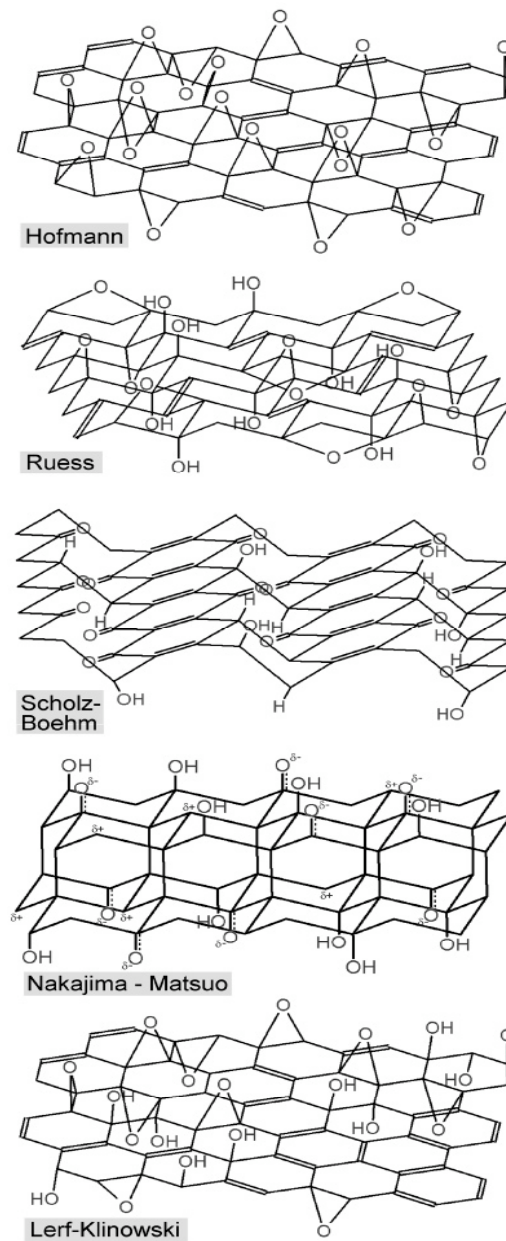


Figure 1: Graphene Oxide. Different theoretical models of graphene oxide displaying epoxide, monoxide, hydroxyl, and carbonyl groups[18].

Because of the thorough oxidation of graphite, the graphene oxide sheets are considered to be insulators[2]. As a result, graphene oxide may also be a useful material as a nanoscale dielectric. Studies show that it may be possible to chemically reduce

graphene oxide back into graphene. Before efficient, large scale production of pristine graphene through chemical reduction is possible, the temperature stability of the oxide needs to be known. The goal of this research project is to determine the reduction kinetics of graphene oxide. This is accomplished by performing TPD measurements which provides information on what compounds are coming of the sample, the activation energy for desorption, and more specifically, to what temperature the oxide is stable.

CHAPTER II

THEORY OF TPD

The process of TPD entails increasing the temperature of a sample under UHV conditions, while concurrently measuring the partial pressures of specific masses. As the temperature of the sample increases, atoms and molecules bound to the surface in a potential well of “ E_{des} ” have an increase in the probability of desorption from the surface. This phenomena is governed by the Maxwell-Boltzmann distribution of statistical mechanics[16].

When a system is in contact with a heat reservoir, at a certain temperature all possible microstates of the system are no longer equally likely. Alternatively, the Boltzmann factor, which goes as

$$e^{-\frac{E}{RT}}, \quad (2.1)$$

biases the distribution towards states with lower energies. The probability of that system having an energy E is described as

$$P(E) = Ag(E)e^{-\frac{E}{RT}}, \quad (2.2)$$

where $g(E)$ is the density of states and A is a normalization constant. Normalizing this function and defining a canonical partition function, Z_c , where a is a microstate, it follows that the probability that a state is in a given microstate is

$$P(a) = \frac{1}{Z_c} e^{-\frac{E}{RT}}, \quad (2.3)$$

where

$$Z_c = \int g(E) e^{-\frac{E}{RT}} dE [15]. \quad (2.4)$$

Furthermore, the canonical ensemble average can be derived from this and is described as

$$\langle x \rangle = \frac{1}{Z_c} \sum_a x(a) e^{-\frac{E(a)}{RT}}, \quad (2.5)$$

where $x(a)$ is a physical property in microstate a , and $E(a)$ is the energy of this state.

Through statistical calculation of $\langle x \rangle$, an equilibrium rate constant of desorption is found and the Arrhenius and Polanyi-Wigner equations are then formulated.

The Polanyi-Wigner equation, shown in equation (2.6), states that the rate equation for the desorption of a gas from a surface in chemical kinetics depends on the concentration of adsorbed molecules per unit surface area N , or coverage, and the temperature T [13].

$$\frac{dN}{dt} = -k_d N^n. \quad (2.6)$$

The derivative of N with respect to time is the rate of desorption, n is the order of the desorption, and k_d is the rate constant. The rate constant is described by the Arrhenius equation, which is acquired from $\langle x \rangle$. The Arrhenius equation, shown in equation (2.7), gives the dependence of the rate constant for a chemical reaction on the temperature and activation energy

$$k_d = \nu_n \exp(-E_{des}/RT), \quad (2.7)$$

where R is the ideal gas constant, T is the temperature, ν is the pre-exponential factor, and E_{des} is the size of the potential well, or the activation energy. Substituting the Arrhenius equation into equation (2.6), it follows that the rate of desorption from a unit surface area may be written as

$$\frac{dN}{dt} = -v_n \exp(-E_{des}/RT)N^n. \quad (2.8)$$

If a linear temperature ramp is used, or $T=T_o+\beta t$ where β is the heating rate, and E_{des} is independent of N , the order of kinetics and activation energies can be derived from the Polanyi-Wigner equation[4]. Taking the derivative of T with respect to time yields

$$\frac{dT}{dt} = \beta. \quad (2.9)$$

Solving for dt and substituting into the Polanyi-Wigner results in

$$\frac{dN}{dT} = -\frac{1}{\beta}v_n \exp(-E_{des}/RT)N^n. \quad (2.10)$$

This is the rate of desorption as a function of temperature and heating rate.

Here, it is suitable to note again that as the temperature of the sample increases, at a certain temperature the distribution of molecules with a thermal energy great enough to desorb from the surface will be appreciable[14]. For the maximum desorption rate at $T=T_m$, the derivative of the rate of desorption with respect to T is evaluated at T_m and set equal to zero, or

$$\frac{d}{dT} \left(\frac{dN}{dT} \right)_{T_m} = 0. \quad (2.11)$$

Noting that the rate of desorption, R_{des} , can be written as

$$R_{des} = -\frac{dN}{dT} = -\beta \frac{dN}{dt}, \quad (2.12)$$

it follows that

$$-\frac{1}{\beta}v_n N^n \left(-\frac{E_{des}}{R} \right) \left(-\frac{1}{T_m^2} \right) e^{-\frac{E_{des}}{RT_m}} - \frac{1}{\beta}v_n n N^{n-1} \frac{dN}{dT} e^{-\frac{E_{des}}{RT_m}} = 0. \quad (2.13)$$

The order of desorption, or order of kinetics, is then determined from the plot of partial pressure versus time by varying the coverage and typically ranges from $0 \leq n \leq 2$.

Zero order, $n=0$, kinetics means that the rate of desorption is independent of the concentration of species, which occurs when species desorb from multilayers. This results in a straight line when the concentration is plotted versus time[4]. A first order reaction, $n=1$, means that T_m is independent of coverage, depends on the heating rate of the sample, and with a constant E_{des} , E_{des} can be calculated directly from a measurement of T_m . With $n=1$,

$$N \frac{E_{des}}{RT_m^2} + \frac{dN}{dT} = 0, \quad (2.14)$$

and it is easily obtained that

$$\ln\left(\frac{Rv}{E_{des}}\right) + \ln\left(\frac{T_m^2}{\beta}\right) = \frac{E_{des}}{RT_m}. \quad (2.15)$$

Noting that $\ln\left(\frac{Rv}{E_{des}}\right)$ is just a constant and rearranging Equation 2.15, an equation of a straight line is then obtained.

$$\ln\left(\frac{T_m^2}{\beta}\right) = \frac{E_{des}}{RT_m} - C \quad (2.16)$$

To calculate the activation energies, a plot of $\ln\left(\frac{T_m^2}{\beta}\right)$ vs. $\left(\frac{1}{T_m}\right)$ is made and the slope of

this graph is (E_{des}/R) . In addition, the y-intercept of this plot is equal to $\ln\left(\frac{Rv}{E_{des}}\right)$. So

with the calculated activation energy, a value for the pre-exponential factor can be obtained. This method of analyzing thermal desorption spectra is known as the Arrhenius plotting method[14].

For a second order kinetic reaction, $n=2$, following similar steps that were done in the first order reaction,

$$\ln\left(\frac{T_m^2}{\beta}\right) = \frac{E_{des}}{RT_m} - \ln\left(\frac{2\nu RN}{E_{des}}\right). \quad (2.17)$$

In this case, our parameters now depend of the surface coverage, N . Surface coverage is obtained from plotting the partial pressure vs. time and calculating the area under the curve. After finding the surface coverage, the activation energy and pre-exponential factor is found in the same fashion as a first order reaction.

Ultimately, the order of kinetics is determined from the behavior of the maximum in the desorption rate curves with coverage. If a change in coverage is made but this does not affect the peak temperature, a first order reaction is assumed. Alternatively, if the coverage is increased, and the peak decreases, a second order reaction is assumed. Second order kinetics exhibit a recombination of molecules on the surface in order for desorption. It is also seen from equation (2.16) and equation (2.17) that to find the activation energy, n doesn't need to be explicitly known, however, n needs to be known to find the pre-exponential factor.

In order to get consistent TPD data, a UHV chamber system capable of supporting a sample mount and manipulator, producing a linear temperature ramp on a sample, measuring the temperature of the sample via thermocouple, and measuring the partial pressures of species coming of the sample is needed. Automation and control of all instrumentation used for the TPD experiment was done by a program written using LABVIEW.

CHAPTER III

EXPERIMENTAL INSTRUMENTATION

A. Quadrupole Mass Spectrometer

In order to acquire accurate measurements of the relative coverage, the partial pressures of the species coming of the sample need to be measured accurately. This was done using a 200 amu quadrupole mass spectrometer (QMS) with electron multiplier, which allows pressure measurements down to 10^{-13} torr. A QMS is also known as a residual gas analyzer (RGA). The QMS first accelerates electrons toward the gas molecules from a filament, which forms ionized gas molecules upon collision with the electrons[17]. An electric field then accelerates the ions from the front of the QMS into the mass selector section, which consists of the RGA probe. The RGA probe contains four parallel metal rods with the two rods opposite of each other having equal and opposite voltages.

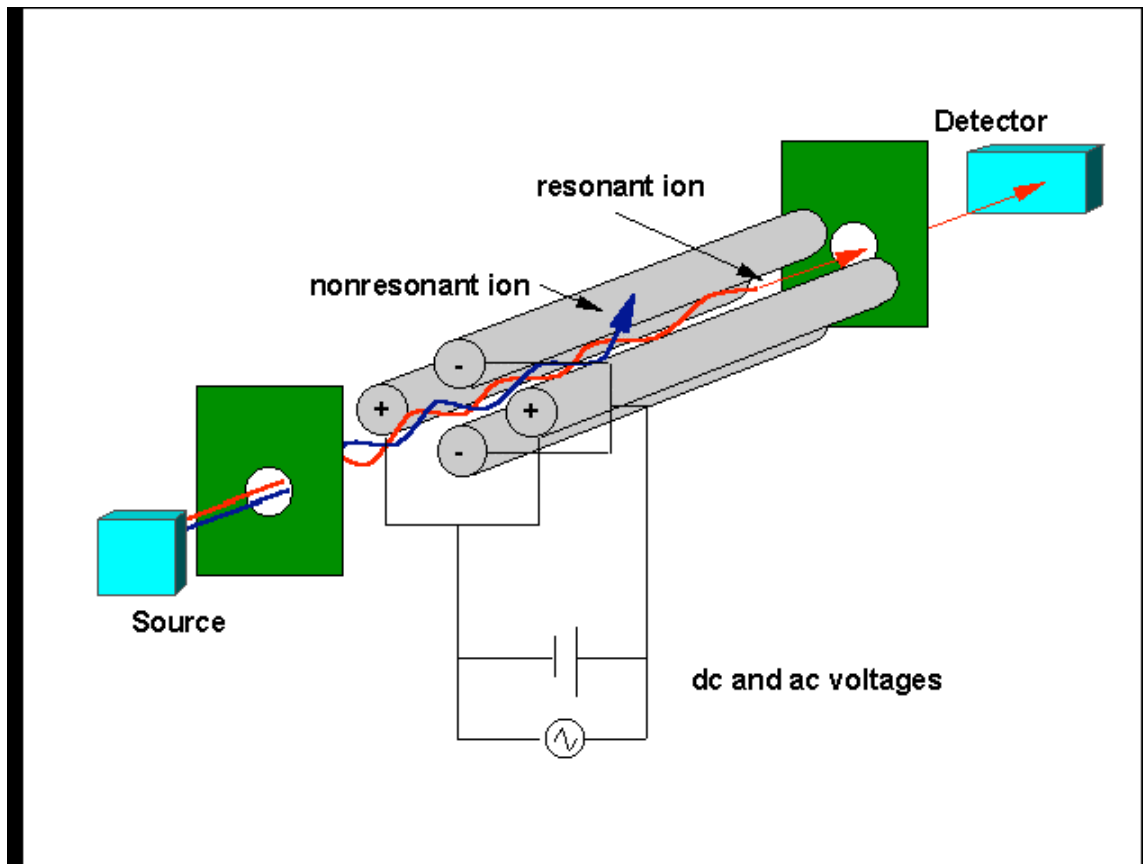


Figure 2: Schematic of RGA probe. Display of mechanics of the mass selection[17]. Notice the creation of the electric field only allowing certain ions to pass.

As the ions pass through the quadrupole field, the voltages of the electrodes are varied using an RF oscillation, allowing only ions with a specific mass to charge ratio (m/z) to pass through to the detector. Varying the RF and DC fields during scanning gives a complete mass spectrum of partial pressures versus mass to charge ratio (m/z)[5]. In addition, after a molecule is ionized, the newly formed molecular ion retains the excess ionization energy. This leads to the molecule fragmenting if the excess energy is greater than the energy required to break a chemical bond. Recording this data gives a good

interpretation of the cracking patterns, which help identify the parent compounds desorbing off the sample. The QMS was mounted on a linear translator that could be moved horizontally 2” so that the intensity of the signal could be enhanced by bringing the QMS within a couple of millimeters of the surface. On the end of the QMS is a shield so that the gases desorbing from the sample are monitored as opposed to the residual gases in the chamber itself or gasses desorbing from the sample holder during the heating process.

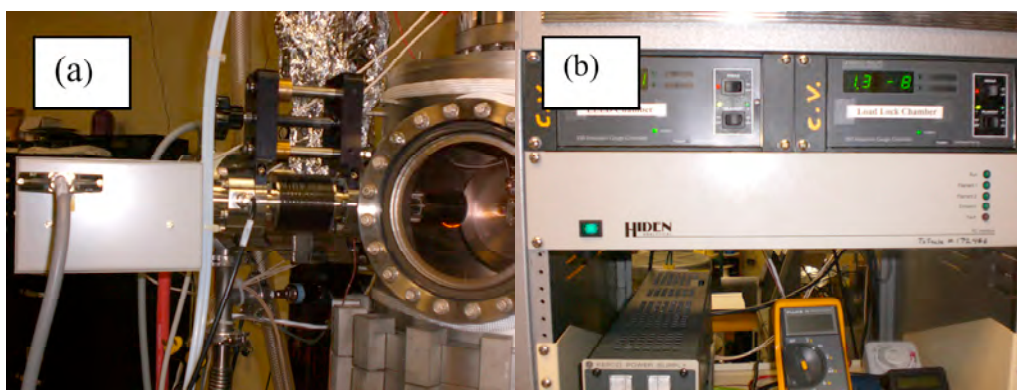


Figure 3: (a)Quadrupole Mass Spectrometer and (b)Interface Unit. Notice that the QMS is mounted on a linear translation so it can be brought closer or farther from the sample.

A programmable Hiden Analytical QMS, HAL 201, was used in this experiment. A program was written to send and receive signals via the RS232 ports on the computer and interface unit (IU). On the front of the QMS IU are five LED's labeled run, filament 1, filament 2, emission, and fault. The LED's indicated whether the QMS was in run mode, which filament was being used, whether the required emission has been obtained, and whether there were any internal faults detected.

B. Load Lock Chamber

Previous TPD experiments with graphene oxide have shown that most of the desorbing gas molecules come off at temperature less than 200 °C. This presents a problem since an integral part of maintaining UHV is the bake out of the chamber. During bake out, temperatures as high as 180 °C are reached so that UHV can be achieved after exposing the chamber to air. A load lock system with magnetic translator was constructed and put on the UHV chamber. This allowed the capability to sustain good UHV pressures and transfer samples in and out of the main chamber without exposing the sample to any detrimental thermal behavior.

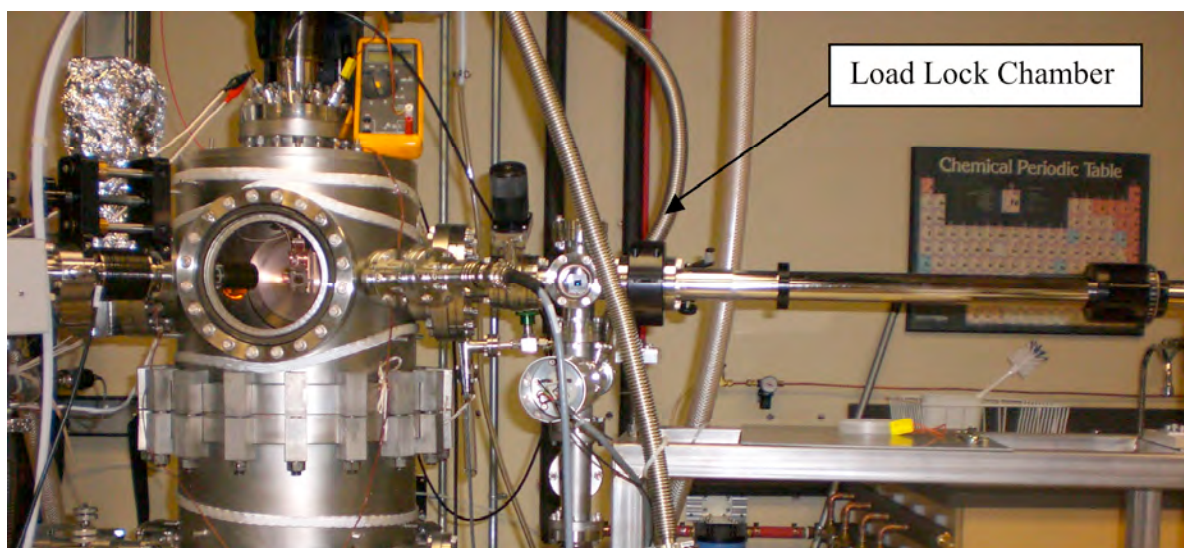


Figure 4: Main Chamber and Load Lock Chamber. Notice the magnetic translator arm on the right of the load lock chamber, which transfers samples to and from the main chamber.

C. Sample Holder and Stage

In order to use the load lock system, a sample holder was machined such that it could be hooked on to the magnetic translator arm, brought into the main chamber from the load lock chamber, and mounted onto the sample holder stage. The load lock system and sample holder system was designed and constructed by Daniel A. Field under the supervision of Dr. Carl Ventrice[19].

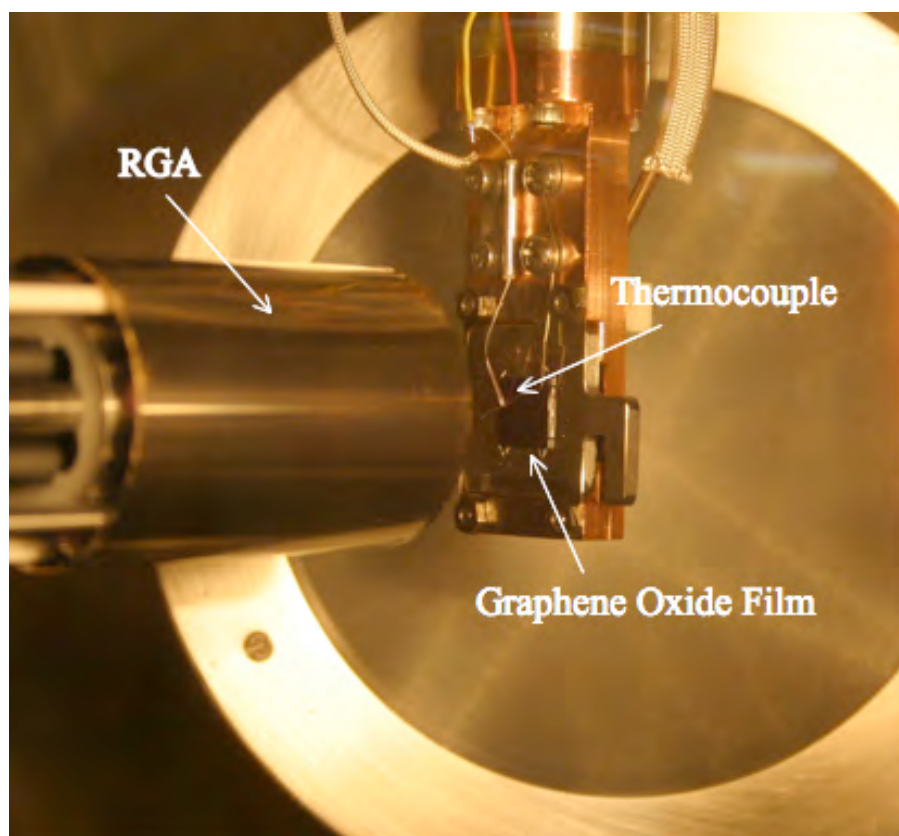


Figure 5: Sample Holder Stage and Thermocouple. Notice the contact made between the tungsten wires and the upon mounting.

As seen in Figure 5, when the sample is mounted on the manipulator, it slides into two molybdenum springs that causes the sample to come into contact with the thermocouple. The thermocouple is used to measure the temperature of the sample, which makes it possible to execute a linear temperature ramp and plot the temperature

versus time and pressure. It works by application of the thermoelectric effect, which says that when a conductor is exposed to heat, it generates a voltage. The conversion from voltage to temperature goes as

$$T = \sum_{n=0}^N a_n v^n, \quad (3.1)$$

where a is just a coefficient, and n ranges from 0 to 9. The type of thermocouple used, categorized by the material used for the junction wire, governs the n value and the coefficients used in the conversion. A chromel-alumel, more commonly referred to as a Type K, was used and the coefficients are listed in the table below[20]:

Table 1: Polynomial Coefficients for K-type thermocouple

n	Type K
0	0.226584602
1	24152.10900
2	67233.4248
3	2210340.682
4	-860963914.9
5	4.83506×10^{10}
6	-1.18452×10^{12}
7	1.38690×10^{13}
8	-6.33708×10^{14}

The voltage signal received from the thermocouple is in the millivolt range. To reduce noise on the signal a pre-amp was used to amplify the signal. The pre-amp was built by Robert Kilbourn. The preamp contained an RC filter with a cutoff frequency of 16Hz and stepped up the incoming voltage by a gain of 100.

The sample was heated by radiative heating from a tungsten filament positioned behind the sample stage. The current through the filament was generated by an ATE 15-6M KEPCO power supply. The control mode of the power supply was such that a 0-1 Volt control signal coming into the instrument produced a 0-6 Amp output current. Therefore, for 1 amp of current, a voltage of .333 volts was sent. In addition, the power supply was set to crowbar mode as a precautionary measure. Crowbar mode allowed the operator to manually turn down the current knob while wired in program mode in case of a programming malfunction. Information being sent and received from the power supply, preamp, and computer, was channeled through a TPD IU using coaxial cables.

D. TPD IU

Enclosed in the TPD IU was a *National Instruments CB-68LPRI/O* connector block. This device has a right angle mounted 68-pin connector whose pins correspond with the input and outputs of the National Instruments Data Acquisition(DAQ) board. On the rear panel of the TPD IU are BNC connectors, which are wired to different analog input/output pins on the connector block, and a 68-pin connector, which connects the TPD IU to the DAQ board installed in the computer. LabVIEW communicated with the instruments using a *National Instruments 6024E* DAQ board. The board has a 12-bit resolution with two analog outputs capable of outputting voltages ranging from 10 to -10 volts. There are 16 single-ended, or 8 differential, analog inputs on the board that have bipolar input signal ranges of 100mv, 1V, 10V, or 20V. The analog inputs and outputs correspond to pin numbers on the connector block in the TPD IU as shown in Figure 6.

AI 8	34	68	AI 0
AI 1	33	67	AI GND
AI GND	32	66	AI 9
AI 10	31	65	AI 2
AI 3	30	64	AI GND
AI GND	29	63	AI 11
AI 4	28	62	AI SENSE
AI GND	27	61	AI 12
AI 13	26	60	AI 5
AI 6	25	59	AI GND
AI GND	24	58	AI 14
AI 15	23	57	AI 7
AO 0	22	56	AI GND
AO 1	21	55	AO GND
NC	20	54	AO GND
P0.4	19	53	D GND
D GND	18	52	P0.0
P0.1	17	51	P0.5
P0.6	16	50	D GND
D GND	15	49	P0.2
+5 V	14	48	P0.7
D GND	13	47	P0.3
D GND	12	46	AI HOLD COMP
PFI 0/AI START TRIG	11	45	EXT STROBE
PFI 1/AI REF TRIG	10	44	D GND
D GND	9	43	PFI 2/AI CONV CLK
+5 V	8	42	PFI 3/CTR 1 SRC
D GND	7	41	PFI 4/CTR 1 GATE
PFI 5/AO SAMP CLK	6	40	CTR 1 OUT
PFI 6/AO START TRIG	5	39	D GND
D GND	4	38	PFI 7/AI SAMP CLK
PFI 9/CTR 0 GATE	3	37	PFI 8/CTR 0 SRC
CTR 0 OUT	2	36	D GND
FREQ OUT	1	35	D GND

NC = No Connect

Figure 6: Pin In/Out of DAQ Board.

CHAPTER IV

EXPERIMENTAL CONTROL AND AUTOMATION

A. LabVIEW

As previously mentioned, all of the experimental control and data acquisition for the TPD measurements was done in *LabVIEW*[22]. *LabVIEW* (**L**aboratory **V**irtual **I**nstrumentation **E**ngineering **W**orkbench) is a graphical user interface programming software used for instrument control and data acquisition. This programming environment uses a dataflow programming language, commonly called G (for graphical programming language), to monitor and control instruments. *LabVIEW* executes code constructed in a graphical block diagram, analogous to the traditional source code, in which the programmer wires together different virtual instruments, or “VI’s”. VI’s can either be a stand-alone program themselves, or be dragged and dropped into the block diagram of another program to be linked to other VI’s, performing the individual sub-functions of a bigger task. Monitoring of the program is done on the Front Panel. The front panel is where the user inputs any parameters and monitors any data being output to a graph or table.

Two programs were written in order to perform TPD measurements. One program performed a linear temperature ramp on the sample while reading voltages from the pre-amp that were converted to temperatures. It was executed through a feedback control loop which first sent out a voltage to the power supply, read in the thermoelectric

voltage of the sample from the pre-amp, converted the data to a temperature, calculated a heating rate, and calculated a new filament current to keep the heating rate constant. While the temperature ramp program ran, the other program simultaneously read in the partial pressures, directly from the QMS IU to the computer, of user-selected species desorbing from the sample. The functionality of the 6024E DAQ board did not allow for all needed task to be run in the same program, so the data from the two programs were output to two separate files and later linked together in the IGOR PRO[21] plotting program by relating the time data from internal clock of the computer, which was stored by each program.

B. MASsoft Professional

Included with the QMS, was software developed specifically for the instrument, *MASsoft Professional*. Communication between the software and QMS IU was done through the RS232 comm port located on the back of the computer tower. This software was used for checking leaks in the chamber and degassing the chamber. Important parameters set by the software are the *operating mode* and the *environment*. The environment is a collection of device settings imposed on the analyzer in order to transport ions from their source to the detector. The *Global* environment was used in this experiment.

The Global environment allows the user to select multiple operating modes, emission parameters, the filament being used, and the type of species. In the Global environment editor, there are two types of detectors the QMS uses that needed to be selected, the Faraday and SEM detectors. The Faraday detector is used when the expected

partial pressures are higher than 10^{-7} torr. Since expected partial pressures in TPD measurements of graphene oxide are much lower, the SEM (secondary electron multiplier) was used, which can measure partial pressures down to the 10^{-13} torr range. The operating mode governs ion acquisition and power consumption of the instrument. The *acquisition mode*, the operating mode used in this experiment, determines what sort of ions will be monitored, and where they originate.

There are different types of acquisition modes dependent upon the type of measurements needed. The RGA mode, in which the analyzer creates ions in an internal electron impact ionization source and extracts positive ions for monitoring, was used in this experiment. Also, to control the power consumption the Shutdown mode was utilized. In this mode, the source emission and SEM supplies are automatically shutdown after a scan. The type of scan wanted is selected under *Scan* mode. To check leaks in the chamber, the QMS was set to *Leak Detect Mode* in which the instrument was assigned to look for a specific gas, helium in our case, and when helium showed up in the chamber, there would be a pressure spike displayed on the pressure vs. time graph on the screen. Before the partial pressure measurement program was opened in LabVIEW, MASsoft was opened in *Profile* mode to degas the filament of the QMS. The Profile mode produces a simple linear mass scan from a user selected starting mass to a stopping mass. In the Profile mode dialog box, the RGA mode, SEM detector, 10^{-10} acquisition range, and scan sweep from mass 2 to 150 amu were inputted. Once the partial pressure vs. mass graph stabilized, the scan was terminated, MASsoft was shutdown, and LabVIEW was opened.

C. LabVIEW-TPD 8-mass measure.vi

In order for LabVIEW to communicate with the QMS IU, ultimately controlling the instrument, Hidden Analytical LabVIEW Instrument drivers and VI's were downloaded from the Hidden Analytical website. These drivers handled all the communication with the instruments and the VI's simplified block diagram design in LabVIEW. The partial pressure measurements were done inside of a while loop, which means that the loop iterates until a boolean condition happens. Outside of the while loop, communication between LabVIEW and the QMS IU is initialized and environment parameters are defined.

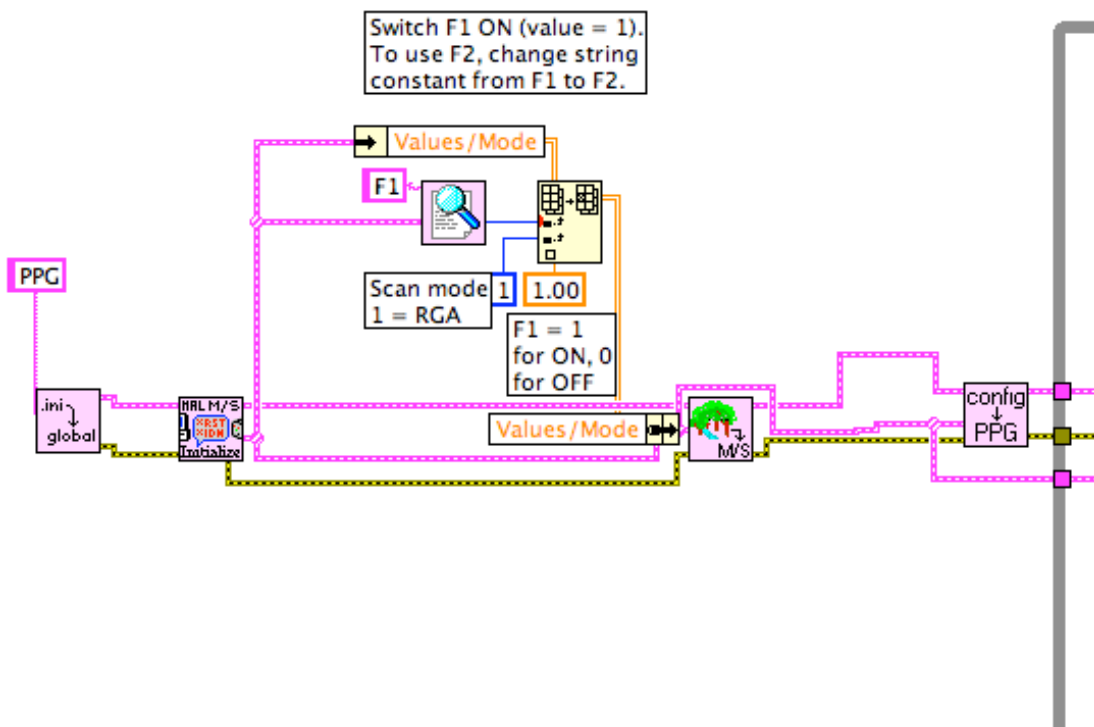


Figure 7: First Execution of Pressure Measurement Block Diagram
Initialization of communication between the QMS IU and LabVIEW.

The block diagram executes code from left to right, so the left most VI will be referred to as the first. The first VI, *Read ini file.vi*, reads the Hiden.ini file to determine the type of communication link, comms link, from LabVIEW to the instrument. Hiden.ini is a file located in MASsoft that interrogates the instruments that are available, meaning that since both software engines will be communicating through the same port, MASsoft and LabVIEW cannot be run simultaneously. The node that “PPG” is wired to configures the Section Name and the VI looks for the PPG comms link in the Hiden.ini file and sends the parameters, in a *cluster*, through the top node to the next VI. The bottom node on the right of the VI is the “error out” link and is connected through all the VI’s, which perform a task and displays any errors in the program upon termination of the loop. The next VI, *HAL Mass Spec Initialize.vi*, opens the comms link to the mass spectrometer, and returns the ID numbers of available instruments and I/O devices. This VI is also capable of outputting a logging file of commands and responses to and from the QMS IU for troubleshooting. This VI must be implemented in order to use any of the instrument drivers for the desired instrument. The nodes from top to bottom on the right side of the VI are the comms link, Mass Spectrometer I/O Devices, and error out link.

In the next section, parameters are pulled out of the cluster, defined, and sent to the *environment download.vi*. The acquisition mode was set to RGA, and Filament 1 was selected. The *environment download.vi* downloads environment data for all the devices and modes supported by the attached mass spectrometer. This data is then wired to the *Hal Partial Pressure gauge configure.vi*. This VI configures the partial pressure gauge by downloading the global environment values from the Mass Spectrometer I/O devices cluster to the QMS IU. This is where the QMS is started, the filament is turned on, and

emission begins, which are all indicated by the LED's on the front panel of the QMS IU. The comms link, error out, and Mass Spectrometer I/O devices clusters are then wired to the *HAL Partial Pressure gauge.vi* on the inside of the while loop through loop terminals. Also wired into the *HAL Partial Pressure gauge.vi* is a cluster that contains all of the scan parameters for an individual mass. The cluster is constructed on top of the while loop and wired down into the scan parameter node of the *HAL Partial Pressure gauge.vi*.

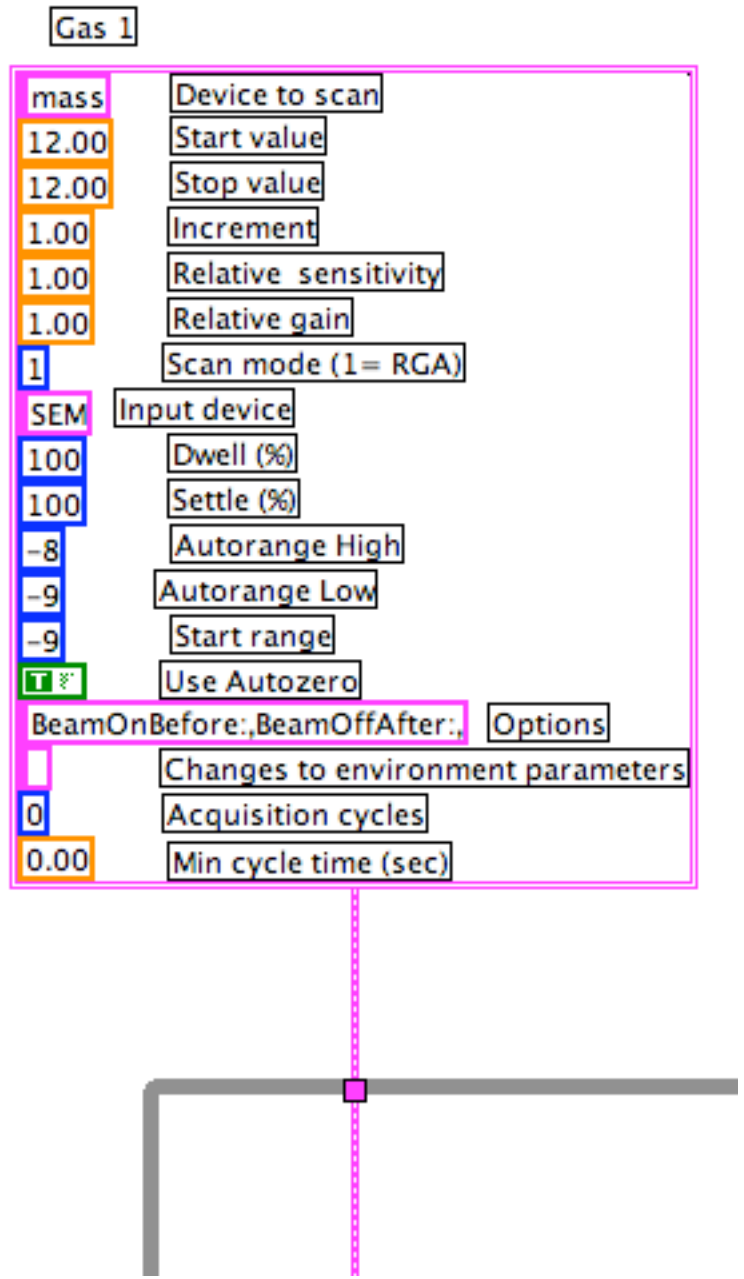


Figure 8: Measurement Parameters . Cluster of measurement parameters that are sent to the QMS IU.

As seen in Figure 8, the first parameters in the cluster define the type of data that the instrument is looking for. The first two text boxes with numerical data define the

start and stopping mass of that individual scan. Since only one mass is required per measurement, the start and stop values are the same. The Dwell, Settle, Autorange High, Autorange Low and Start range textboxes all work in conjunction with each other. The QMS detector is able to measure of a large range of pressures, which is executed by switching pressure ranges. Upon taking a measurement, the QMS sets whatever devices it needs to adjust, waits for the settle time, and then takes a reading by averaging over the dwell time. In order to keep the signal to noise ratio consistent, the detector changes its settle and dwell times to be suitable for the range its on.

The detector has in internal table of settle and dwell times from which it chooses acceptable signal to noise ratios for the different ranges. Setting the dwell and settle to 100% allows the full dwell and settle times from the internal table, allowing more time for more sensitive readings, thus resulting in a more accurate partial pressure measurement. If the range of a species is known, the range that the detector uses can be restricted to an upper and lower limit, thus giving a shorter dwell and settle time. The autozero parameter governs whether an absolute partial pressure reading is returned (T-True), or a difference in partial pressure measurement is returned (F-False). The 'BeamOnBefore:,BeamOffAfter' sends a command to the instrument to turn the ion beam on, and then after the measurement turn the beam off. This cluster is called when the VI to which it is wired begins execution. The first section within the while loop contains the *HAL Partial Pressure gauge.vi* and the *HAL Mass Spec format display data.vi*.

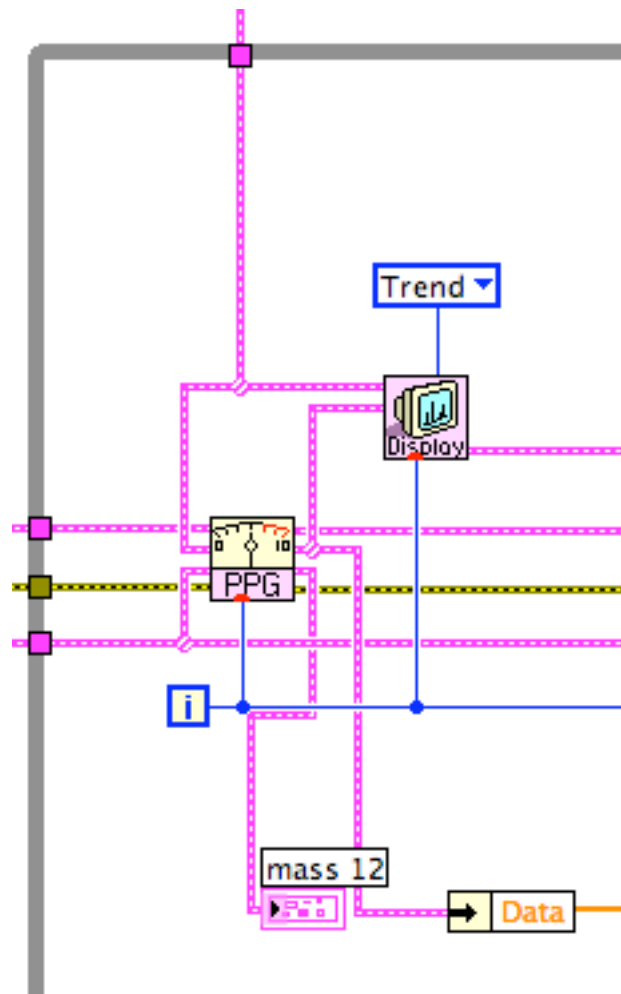


Figure 9: First Execution Inside While Loop of Pressure Measurement. VI labeled “PPG” is the *Partial Pressure gauge.vi*. Executes the actual pressure measurement.

Using the clusters wired into it, the *Partial Pressure gauge.vi* is where the partial pressure measurement is done. First, it sends the operating mode and species to be measured to the instrument, turns on the ion beam, and waits for the measured value to return from the selected input device. After the value returns, if it is out of range, the VI changes the Input device range until the reading is in range or the defined autorange is reached. When an acceptable value is measured, it is returned to the VI and the ion beam is turned off. The two middle nodes on the right side of the VI outputs the acquired data

in clusters. The node second from the bottom is wired to an indicator that outputs the data cluster to the front panel. In this cluster of data is the “Measured data”(partial pressure,) “Set data”(mass of species), “M.D. units”(torr), “S.D. units”(amu), and Boolean signals that control LED’s that light up when a signal is under or over range.

Also included in this cluster, is the elapsed time, which is relative to the time at which the *Hal Partial Pressure gauge configure.vi* was executed. The node second from the top outputs the same data cluster, except in the form of an array. This array is sent to the *HAL Mass Spec format display data.vi*. This VI takes the incoming data array and formats it for display on a graph on the front panel either as a linear display vs. the scanned parameter or as a trend display vs. elapsed time. It also takes the scan parameters cluster and uses it to label the graph axes and legend. The cluster from this node is also branched off to a property node that pulls out the measured data for later manipulation. To obtain more mass measurements, this section was repeated seven more times and wired together in series so that measurements were taken sequentially(refer to Appendix A). Once the last measurement section is configured, to output all the partial pressures to the front panel versus time, modifications to the final *HAL Mass Spec format display data.vi* were made.

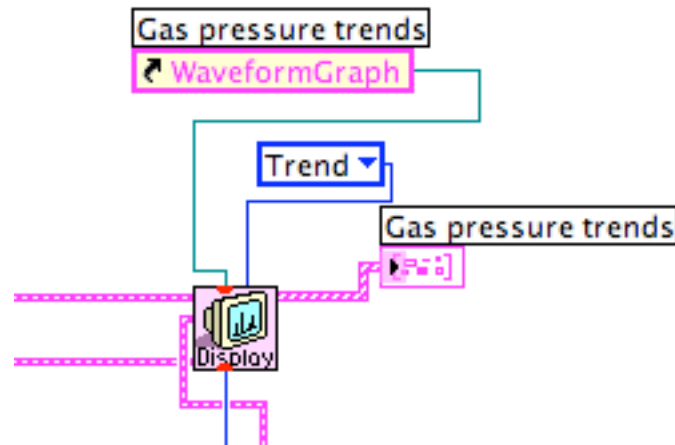


Figure 10: Data Formatting. VI labeled “Display” is the *HAL Mass Spec format display data.vi*. Executes data formatting for display on front panel.

Display data are sent through the preceding *HAL Mass Spec format display data.vi*'s through the bottom node on the left and right sides, “Display link in/out”.

Across the top of the VI are where the type of graph wanted is wired in. On the right side of the VI the top node, “XY Graph data”, sends the array of information to an indicator that displays a graph on the front panel. While data are being displayed to the graph, there is also a table on the front panel that updates every iteration with numerical values of the partial pressure of each mass. It receives its values from an array that was built with the contents of the property nodes pulling out the measured data. During run-time, measured data and other parameters are monitored on the front panel. In addition to being sent to a front panel table, this array is appended with the time of the internal clock of the computer, sent to an array builder that compiles the array from every iteration and written to a file indicated by the user. Upon termination of the while loop, the Comms Link, Mass Spectrometer I/O devices, and error message clusters are sent to the *HAL Mass Spec Close.vi*, which is outside of the loop.

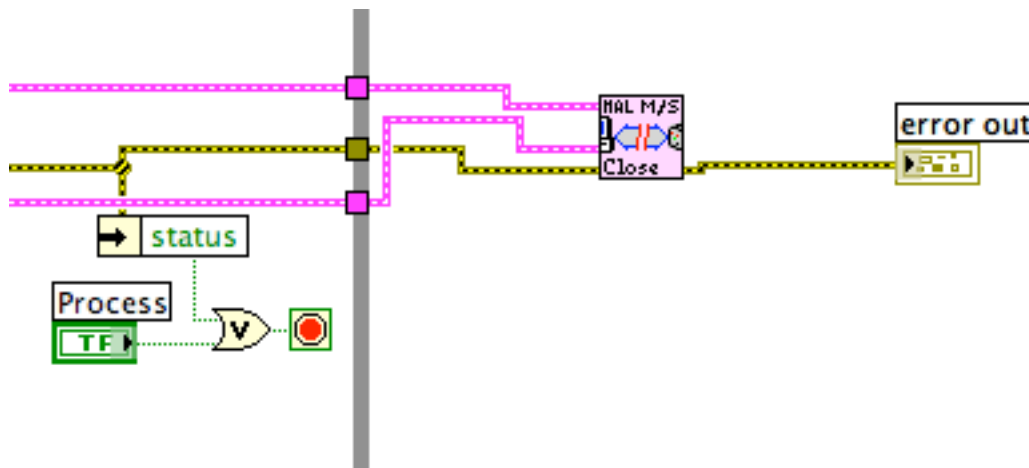


Figure 11: Last Execution of Pressure Measurement Loop. VI labeled “HAL M/S Close” is the *HAL Mass Spec Close.vi*. Required upon termination of loop.

When executed, this VI stops the scan, turns off the filament, and turns off the emission, as indicated by the QMS IU LED’s. It sets the instrument to standby mode, discontinues communication to the instrument, and writes the current QMS configuration and values to a file for troubleshooting.

D. LabVIEW-TPD RAMP.vi

This program was also based around a while loop, more specifically, a feedback control loop. Outside of the while loop are the controls for the Voltage output channel, Initial Current, and Total Time.

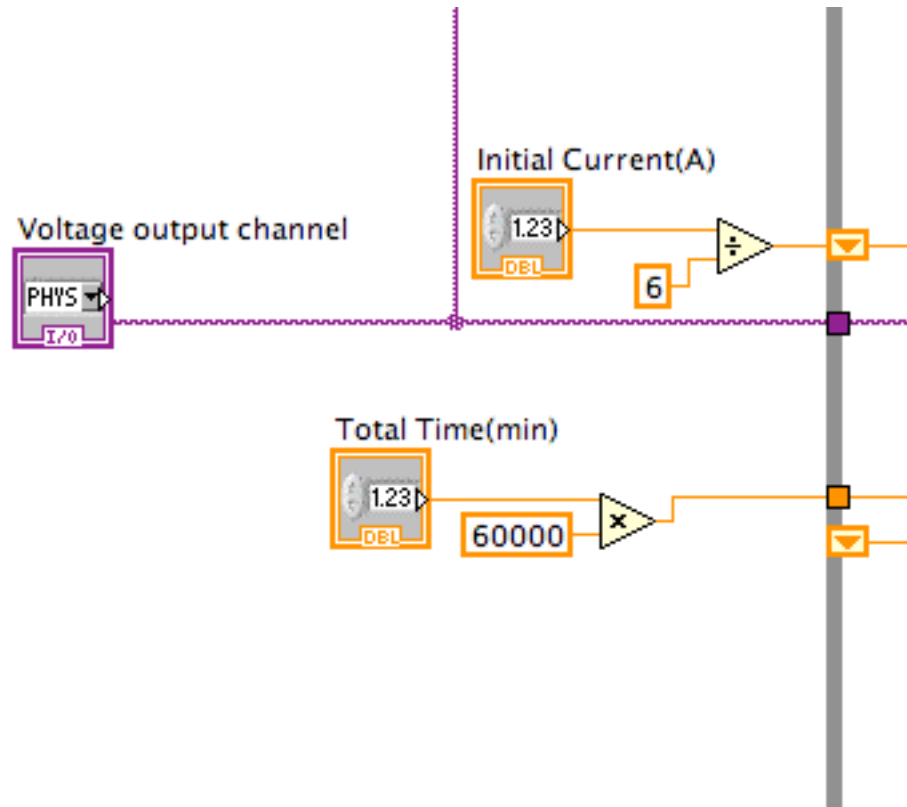


Figure 12: First Execution of Temperature Ramp. These controls call user inputted data from the front panel.

The Initial Current is wired into a math operator that divides it by six because LabVIEW sends a voltage to the power supply that then sends the desired current to the filament, and as mention earlier, there is a 6 to 1 conversion factor from amperes to volts. After the Initial Current is converted, it is wired to a shift register on border of the while loop. After the first iteration, the shift register updates the parameter to the value that is

contained in the corresponding shift register at the end of the while loop. The Total Time is converted to milliseconds because inside the loop all timing parameters will be in the units of milliseconds.

Inside of the while loop, there is a true/false case structure. If a true statement is sent to the case structure, the current is not updated and is held at the initial current. If a false statement is sent, the current is updated every iteration.

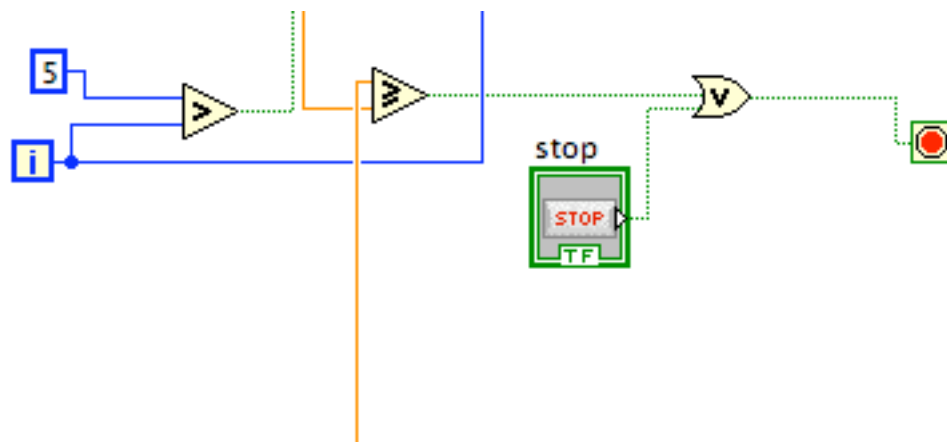


Figure 13: Comparison Conditions. Governs which case structure executes and termination.

This is done so that the first few seconds of the run, the temperature of the sample can “catch up” to the heat it’s receiving from the filament. As seen in Figure 13, if the number of iterations is less than five, a true statement is sent to the case structure and the code for this case is then executed. Also in Figure 13, are the stopping conditions. The greater than or equal to sign compares the inputted Total Time with the time from an elapsed timer located elsewhere in the loop. The while loop terminates upon a true statement being sent from the comparison or when the stop button, positioned on the front panel, is pressed.

Inside of the TRUE case structure there is a flat sequence structure. This is needed so that the order of operation of the code is executed sequentially. In the first sequence, the incoming current is compared to the final current parameter and if the incoming current is less than the final, the current value is passed, and if it is greater, the final current is passed. In the next sequence, a voltage is sent to the power supply.

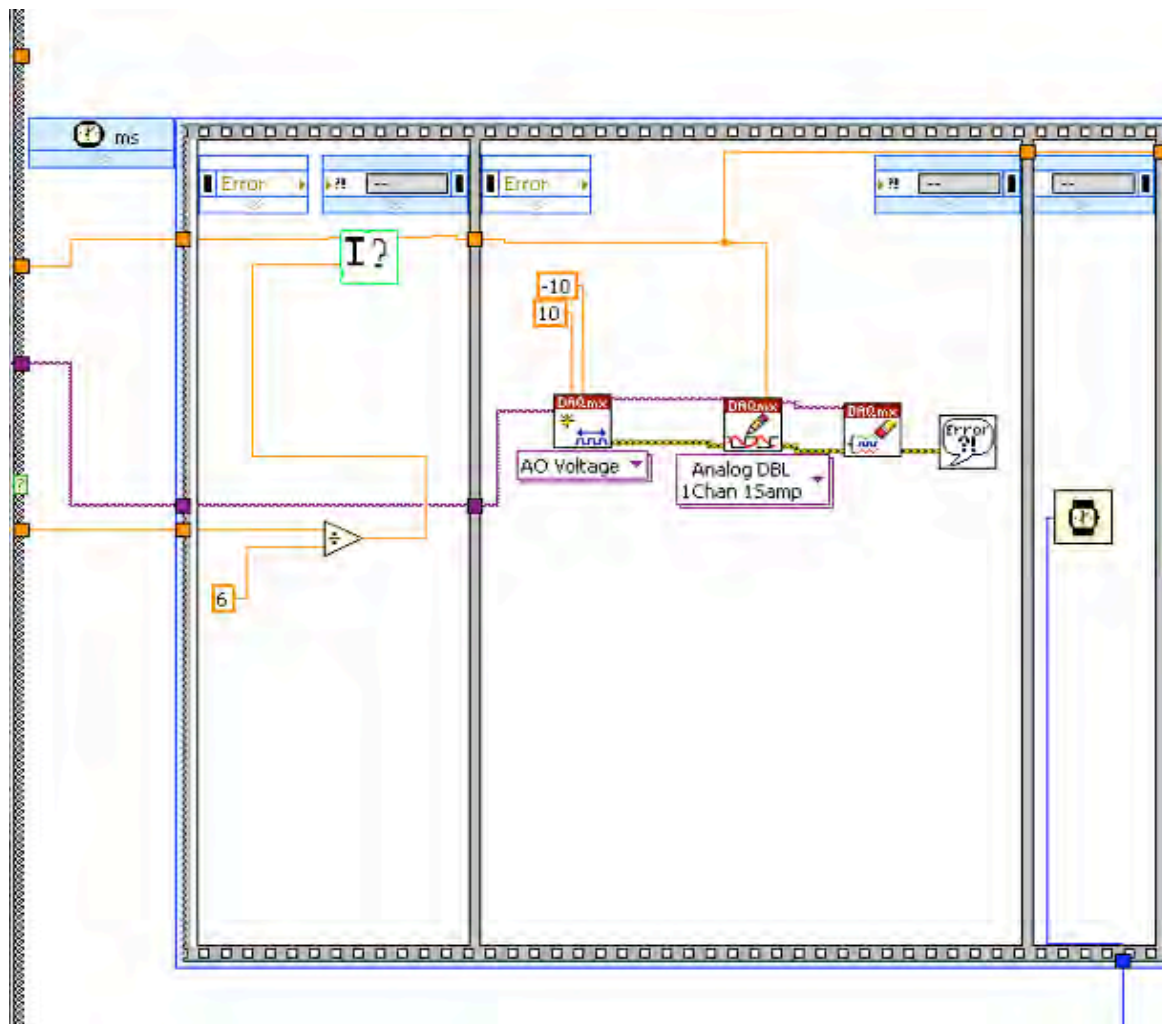


Figure 14: First Sequences in True Case Structure. Executes current check and voltage output.

The first VI, *DAQmx Create Virtual Channel.vi*, starts the communications with the user selected output channel and sets the programmable bipolar voltage range with the values wired into the nodes across top edge of the VI. After the channel is activated, the *DAQmx*

Write.vi sends the desired voltage to the output channel. The next VI, *DAQmx Clear Task.vi* clears the task that was created with the *DAQmx Create Virtual Channel.vi*, which helps to avoid allocating unnecessary memory. The next sequence executes the dwell time inputted by the user. The purpose of this dwell time is to allow the sample enough time to respond to the current being sent to the filament. As will be discussed later, if this dwell time is absent, the temperature measured in the next sequence will not be an accurate measure of temperature induced by the current that was just sent.

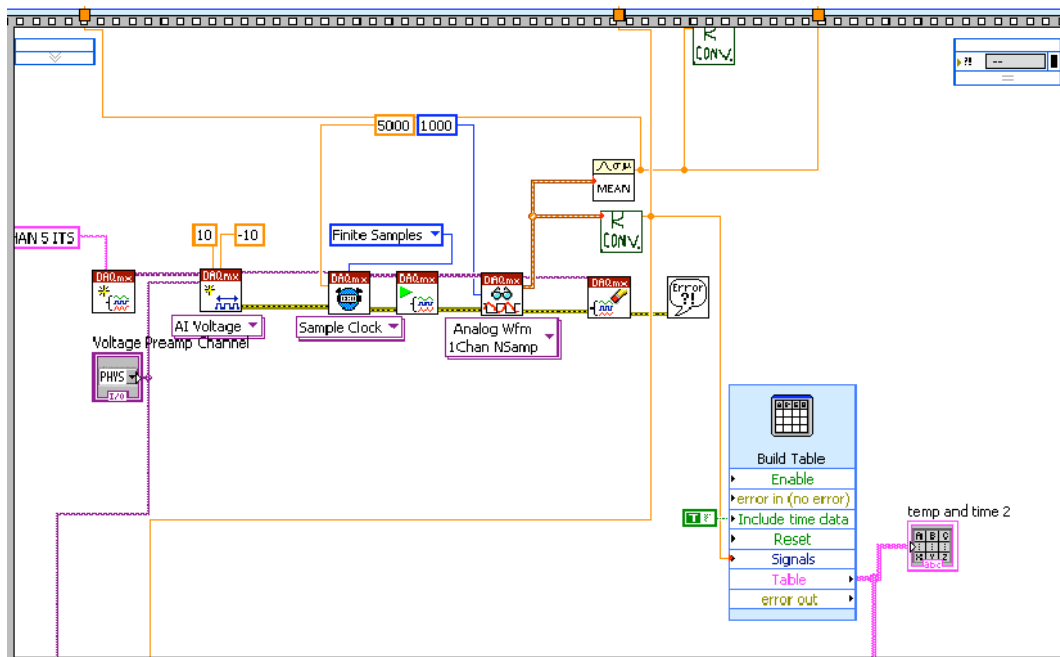


Figure 15: Fourth Sequence in True Case Structure. Voltage Acquisition.

The fourth sequence of the case structure executes the data acquisition portion of the loop. Here, the *DAQmx Create Virtual Channel.vi* designates the user defined input channel as an analog voltage input. The *DAQmx Read.vi* where the voltage reading from the thermocouple is executed. The user specifies what format of samples to return, whether to read a single sample or multiple samples at once, and whether to read from

one or multiple channels. The measurement is then sent to the *K CONV.vi* where it is inserted into the formula that converts a voltage to temperature for a K-type thermocouple using the values from Table 1. After the conversion to temperature is done, the value is then sent to a table that displays the value on the front panel, a graph that plots temperature vs. time, and various other places throughout the program. This was the last sequence in the TRUE case structure.

Outside of the case structure an elapsed timer displayed the elapsed time on the front panel in minutes and seconds. In addition, the *Get Date/Time In Seconds.vi* retrieved the time from the internal clock of the computer outside of the case structure, and this time stamp along with the measured temperature were wired to Auto-Indexed tunnels on the right border of the while loop so that arrays of these values could be built. The elapsed time, measured temperature and voltage sent to the power supply were wired to shift registers on the right border of the loop so that these values could be passed through to the next iteration of the loop. On the sixth iteration of the loop the FALSE case structure was called. This case structure executed the same four sequences of the TRUE case structure first, and then executed two more sequences that added the code for feedback control.

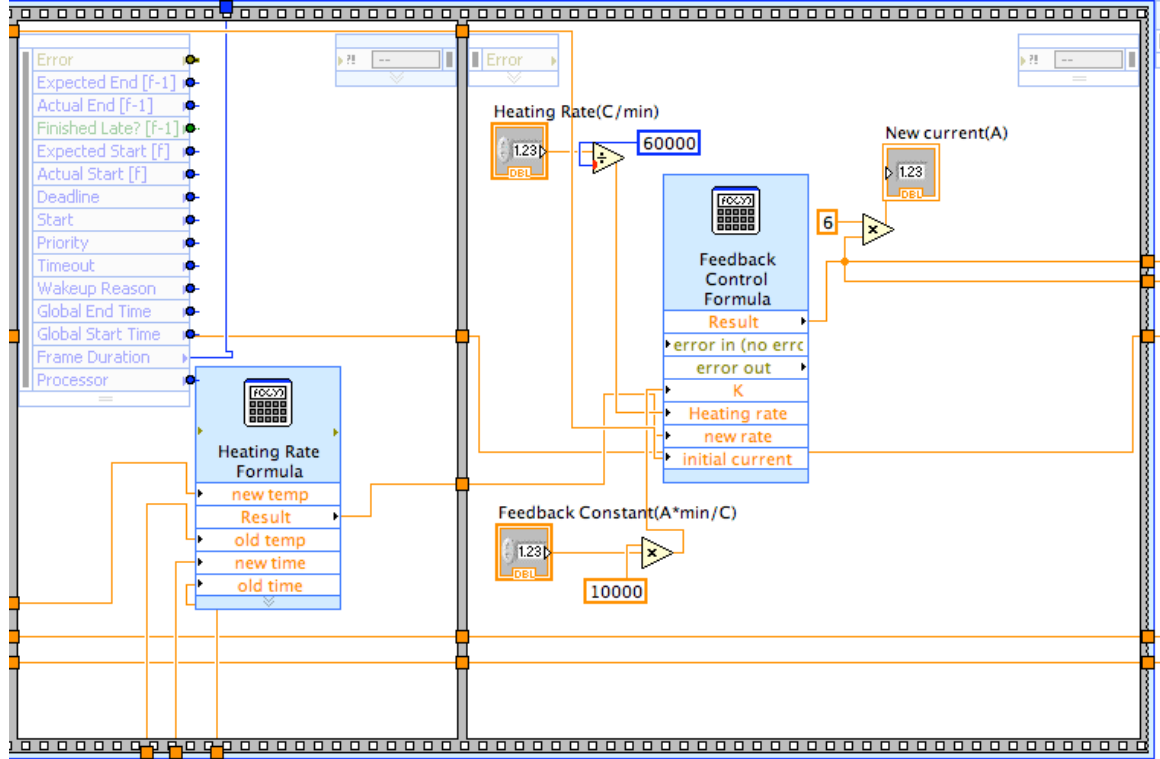


Figure 16: Final Sequences of False Case Structure. Executes feedback control portion of loop.

In the left sequence, the heating rate was calculated. The new temperature, the temperature iteration, elapsed time, and elapsed time from the previous iteration were input into the *Heating Rate Formula.vi*. This VI implemented the following formula:

$$\frac{\Delta T}{\Delta t} = \frac{T_n - T_{n-1}}{t_n - t_{n-1}} = R_{h_n} \text{ (}^\circ\text{C/ms)}, \quad (4.1)$$

where n is the current iteration, T is the temperature, t is the elapsed time, and R_h is the heating rate. This heating rate is then passed through to the next sequence. This sequence uses a feedback control formula to calculate a new current that would give the desired heating rate. The *Feedback Control Formula.vi* implements the following formula:

$$k(R_h - R_{h_n}) + I_n = I_{n+1}, \quad (4.2)$$

where k is the feedback proportionality constant, and I is the current being sent to the filament. First, the desired heating rate, which is input by the user in ($^{\circ}\text{C}/\text{min}$), is converted to ($^{\circ}\text{C}/\text{ms}$) and k , which is input by the user in ($\text{A}\cdot\text{min}/^{\circ}\text{C}$), is converted to ($\text{V}\cdot\text{ms}/^{\circ}\text{C}$). These values, along with I_n and R_{h_n} are then called by the *Feedback Control Formula.vi*. If the current heating rate higher than the desired heating rate, the parenthesis results in a negative value, which then is multiplied by the proportionality constant, also positive. This value is then added to the voltage that was sent to the power supply, which results in a new voltage that is lower than the previous one. If the current heating rate is lower than the desired heating rate, the new voltage is increased. The new voltage is then passed through to the shift register that updates the voltage being sent to the power supply. After this sequence executes, the loop iteration is done, and as previously mentioned, the while loop continues to iterate until the Total Time is reached, or the stopped button is pressed.

Upon termination, the user is prompted for a file destination and the arrays built are manipulated and output to the file chosen for data analysis.

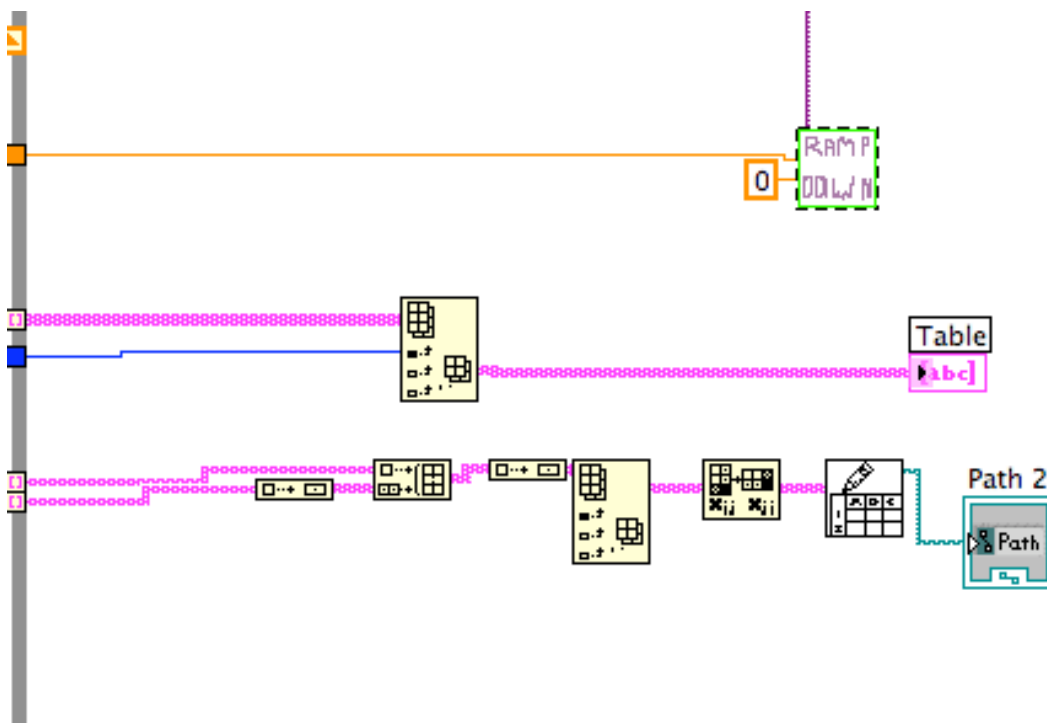


Figure 17: Last Execution of Temperature Program.

After the arrays are output to the file destination, the *Ramp Down.vi* begins execution.

This VI slowly ramps down the voltage being sent to the power supply.

CHAPTER V

RESULTS

A. Sample Preparation for Measurement

TPD was performed to obtain desorption kinetics and activation energies in the chemical reduction of graphene oxide. Thin films composed of graphene oxide platelets were used in the analysis. The samples were prepared by Dr. Rod Ruoff's group at the University of Texas-Austin by depositing droplets of aqueous solution of graphene oxide onto Si(100) substrates with 300 nm silicon dioxide overlayers. Graphene oxide platelets were formed by two methods of exfoliation of graphite oxide. The first method, ultrasonication, resulted in an average platelet size of 1 μm . Using ellipsometry, after depositing ultrasonicated platelets on the sample substrate, an average multi-layer graphene oxide film of thickness 35.9 nm was determined. The second method, slow-stirring, resulted in an average platelet size of 10 μm . After deposition, the film thickness was found to be 8.5 nm.

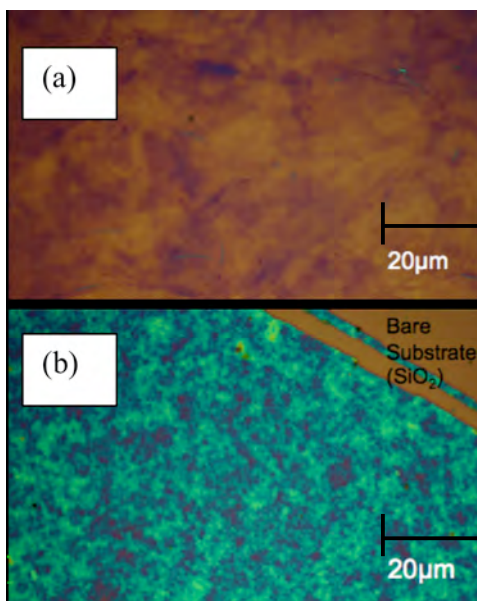


Figure 18: Optical Image of Films. Top film represents (a) slow-stirred graphene oxide. Bottom film represents (b) ultrasonicated film.

The samples were then mounted onto the sample holder by placing them over the hole, and spot welding four wires over the corners of the sample (see Figure 5). The sample holder was then placed in the load lock chamber and the chamber was pumped down with a mini turbo pump. Once the load lock chamber reached a vacuum of 10^{-7} torr, the sample was transferred into the main chamber. During heating of the sample, compressed air was sent into the dewar assembly at the top of the chamber to act as a cooling mechanism for the thermally sensitive parts of the sample stage. At this point, the MASsoft program was started to degas the QMS.

B. Pressure Program Preparation

The partial pressures of the masses 12, 14, 16, 17, 18, 28, 32 and 44 were measured with the pressure measurement program. These masses were analyzed due to the importance of obtaining the activation energies and desorption kinetics of compounds containing carbon, hydrogen, and oxygen. Large concentrations of compounds containing hydrogen and oxygen are expected because of the original oxidation process of the source graphite material and the subsequent exfoliation in deionized water. Masses 18, 28, 32, and 44 correspond to compounds H₂O, CO, O₂, and CO₂. Masses 12, 14, 16, and 17 were measured because they are cracking fragments of the desorbing compounds. Since each desorbing molecule has its own relative sensitivity, minimum and maximum autorange values were obtained so that there was minimal dwell time between readings. Without these values being implemented into the program, with the dwell and settle percentages set to 100%, the QMS detected over the full range of the SEM and this resulted in dwells up to seven seconds, causing inconsistencies with the data collection. A table of the estimated ranges of each specific mass is found in Table 2.

Table 2: Autorange Values of Each Respective Mass

MASS(amu)	Autorange High(torr)	Autorange Low(torr)	Start range(torr)
12	10 ⁻⁸	10 ⁻⁹	10 ⁻⁹
15	10 ⁻⁹	10 ⁻⁹	10 ⁻⁹
16	10 ⁻⁸	10 ⁻⁹	10 ⁻⁹
17	10 ⁻⁸	10 ⁻⁹	10 ⁻⁹
18	10 ⁻⁷	10 ⁻⁹	10 ⁻⁹
28	10 ⁻⁷	10 ⁻⁹	10 ⁻⁹
32	10 ⁻⁹	10 ⁻⁹	10 ⁻⁹
44	10 ⁻⁷	10 ⁻⁹	10 ⁻⁹

With these values the average runtime of each iteration was 1.7 seconds. In addition to affecting the dwell time of the measurements, the relative sensitivity also affects the partial pressure measurements of each mass. Therefore, in data analysis, the partial pressures were corrected for the ionization efficiency of the molecules.

C. Temperature Ramp Program Preparation

On the front panel of the temperature ramping program, the user inputs the wanted heating rate($^{\circ}\text{C}/\text{min}$), maximum current(A), initial current(A), total run time(min), dwell time(ms), and proportional feedback constant($\text{A} \cdot \text{min}/^{\circ}\text{C}$). Three different heating rates of $50^{\circ}\text{C}/\text{min}$, $25^{\circ}\text{C}/\text{min}$, and $10^{\circ}\text{C}/\text{min}$ were used for analysis of both the ultrasonicated and slow-stirred films. In order to protect the filament from failing, the maximum current was set to 4 A. The temperature of the sample didn't significantly respond to the filament until a value of about 2 A was achieved, so the initial current was set to 1.7 A. The total runtime was dependent upon the heating rate of the run. The runtime had to be long enough so that temperatures up to 300°C were attainable, which gave a full spectrum of the desorbing molecules. The linearity of the ramp depended heavily on the next two values. The k value controls the deviation from the current of the previous iteration. Therefore, if k is too small the updated current will produce a new current that is similar to the current from the previous iteration resulting in a logarithmic, instead of linear, growth in temperature. If k is too large and the current needs to be decreased, the formula will undershoot the value. Conversely, if the current needs to increase the formula will overshoot the value and these two events result in an oscillation of the temperature versus time plots. The amplitude of the oscillation depends on how big the k value is in addition to the dwell time. As previously mentioned, if

the dwell time is too short, the DAQ board isn't given enough time to read the response to the change in current. Conversely, the larger the dwell time, the longer the sample has to undergo the logarithmic increase in temperature. Therefore, a large correction will be needed to correct the current, resulting in full amplitude of oscillation.

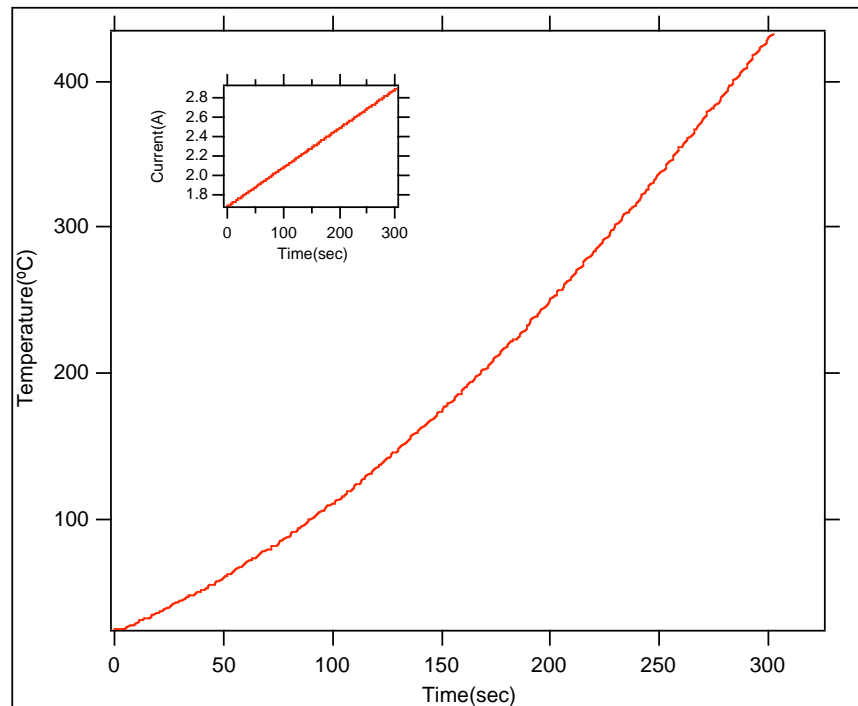


Figure 19: Ramp with Linear Current Increase. Notice the effects on the temperature ramp with a linear increase in current.

The importance of using a feedback control system is shown in Figure 19. If the current is incremented linearly, the heat transfer from the filament to the sample is governed by the Stefan–Boltzmann law. This law states that the energy, or power of energy, radiated by a blackbody radiator per second per unit area is proportional to the fourth power of the absolute temperature.

$$P = jA = A\epsilon\sigma T^4 \quad (5.1)$$

The power is directly related to current in the filament by $P=I^2R$. After a polynomial fit was performed, it is shown experimentally and by the Stefan-Boltzman law that as current is linearly increased, temperature is quadratically increased by a power of two.

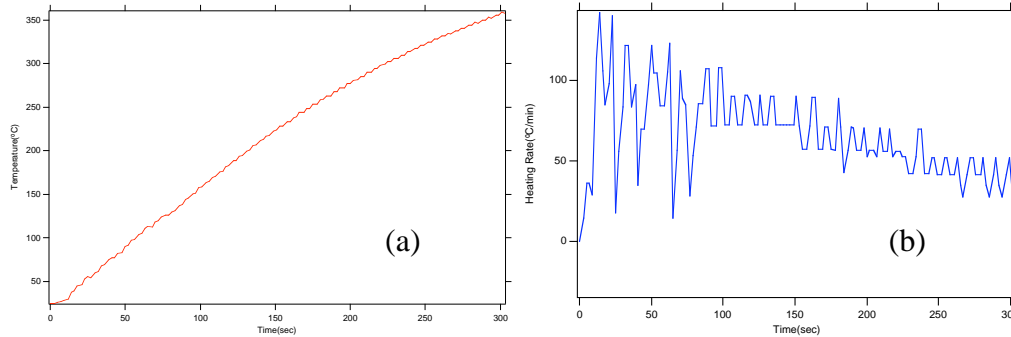


Figure 20: Ramp with Varied Parameters-1.(a) Temperature vs. Time curve. (b) Heating Rate vs. Time curve. Notice the effects on the temperature ramp with large k value.

The temperature vs. time, and heating rate vs. time curves for a temperature ramp with $k=0.9$, $R_h=50$, and $dwell=2$ sec are shown in Figure 20. These parameters caused small oscillations in the temperature vs. time curves and also caused the curve to render more of a logarithmic function rather than a linear function. For the safety of the filament, current being sent to the filament was leveled off at 3.2 A, so the oscillations on the temperature vs. time graph are not extreme, but it seen in the heating rate vs. time curve the large affects of the varied parameters. Nominally, it is expected that the slope of the heating rate vs. time curve should be relatively close to zero in order to achieve a linear increase in temperature. However, when the derivate of temperature with respect to time is taken and plotted against time, a slope of -0.16 ± 0.02 .

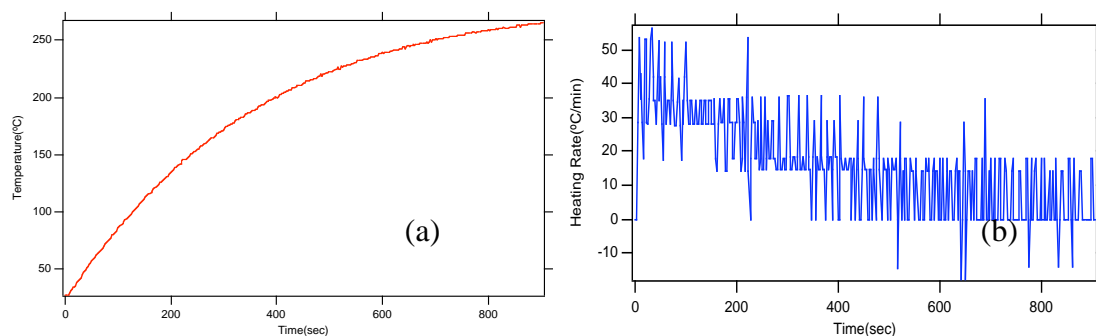


Figure 21: Ramp with Varied Parameters-2. (a) Temperature vs. Time. (b) Heating Rate vs. Time curve. Notice the effects on the temperature ramp with small k value.

The result of when the k value is too small is shown in Figure 21. Here, a k value of 10^{-5} , a heating rate of $50\text{ }^{\circ}\text{C}/\text{min}$, a dwell of 2 sec were input into the program. By letting the program run for 15 minutes, it is easily seen that the temperature vs. time curve resembles a logarithmic function. The curve levels off because the energy being radiated from the filament isn't enough to produce an increase in temperature, thus the temperature levels off at $260\text{ }^{\circ}\text{C}$.

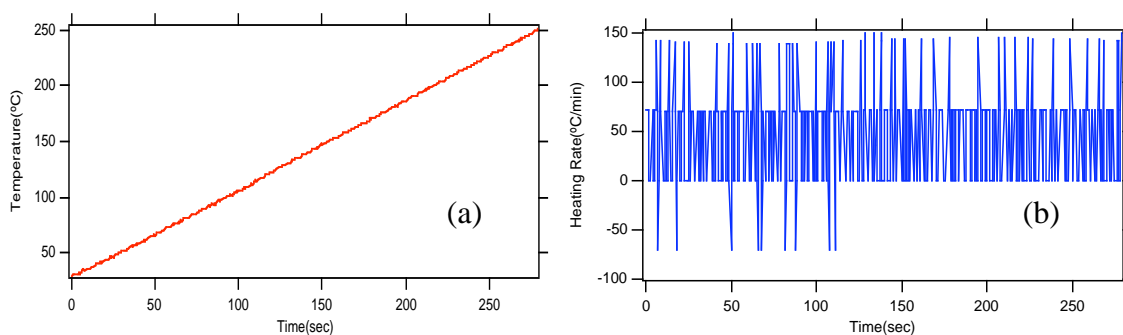


Figure 22: Linear Temperature Ramp. (a) Temperature vs. Time curve. (b) Heating Rate vs. Time curve.

Through testing and manipulation of the parameters, consistent linear temperature ramps were achieved, as shown in Figure 22. It was determined that a k value of 0.0015 and a dwell of 500 ms produced a linear heating ramp for $R_h=50\text{ }^{\circ}\text{C}/\text{min}$. The slope of the

temperature vs. time was calculated to be 0.79789, which after converted to °C/min corresponded to a heating rate of 47.9 °C/min. The slope of the heating rate vs. time curve is 0.017, which is fairly close to zero and thus depicts a constant heating rate. For the heating rates of 25 and 10 °C/min, the dwell time that gave consistent linear heating ramps was also 500 °C/min.

D. Analysis of TPD Spectra

1. $R_h=50^\circ\text{C}/\text{min}$

Partial Pressure vs. Temperature Curves for $R_h\sim 50^\circ\text{C}/\text{min}$

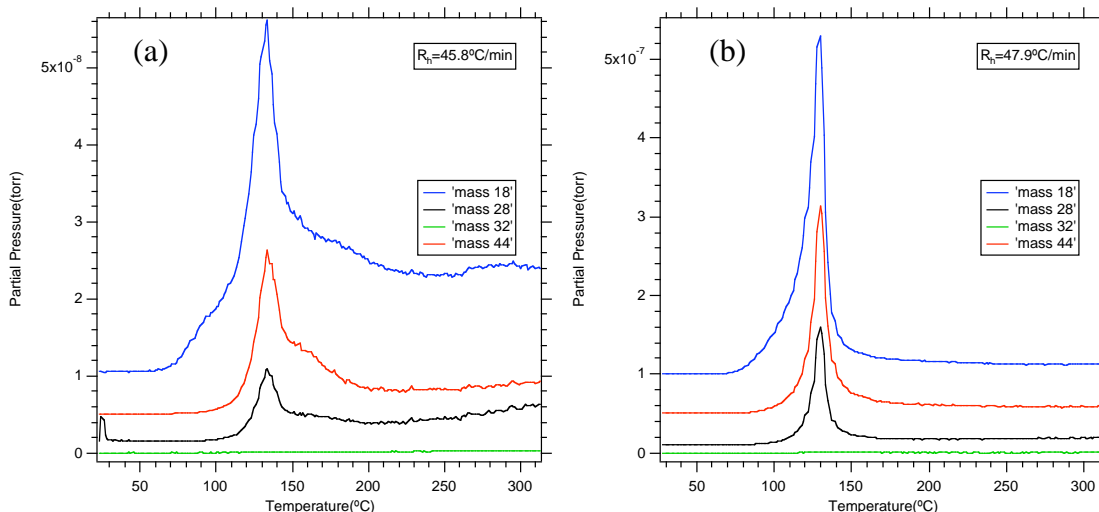


Figure 23: Partial Pressure vs. Temperature Curves for $R_h\sim 50^\circ\text{C}/\text{min}$. (a) slow-stirred (b) ultrasonicated.

Spectra obtained for the slow-stirred and ultrasonicated films at a heating rate of $\sim 50^\circ\text{C}/\text{min}$ is shown in Figure 23. The corrections for the ionization efficiencies were made using the table of *Cracking patterns for gases and vapours* from Hiden Analytical (refer to Appendix B). In addition, there was also another correction made to mass 28 in all the spectra. CO is a cracking pattern of CO_2 , therefore, the amount of CO that the QMS is detecting also includes the amount that could be a fraction of CO_2 . To account for this the cracking component of CO_2 that is CO was subtracted from the measured CO peak. There is a CO peak detected in the beginning of the spectrum, and as will be seen later this same peak is fairly consistent in all spectra. It is determined that this peak is caused by the emission from the start up of the filament. For the both films, the masses with the largest peaks were 18, 44, and 28, which correspond to H_2O , CO_2 , and CO molecules. For the slow-stirred film,

the peak temperature of these molecules was found to be at 133 °C. Desorption began at 70 °C and proceeded to 220 °C. For the ultrasonicated film, the peak temperature was found to be at 129 °C. Desorption of molecules began at 80 °C and was completed by 170 °C.

2. $R_h=25\text{ }^\circ\text{C}/\text{min}$

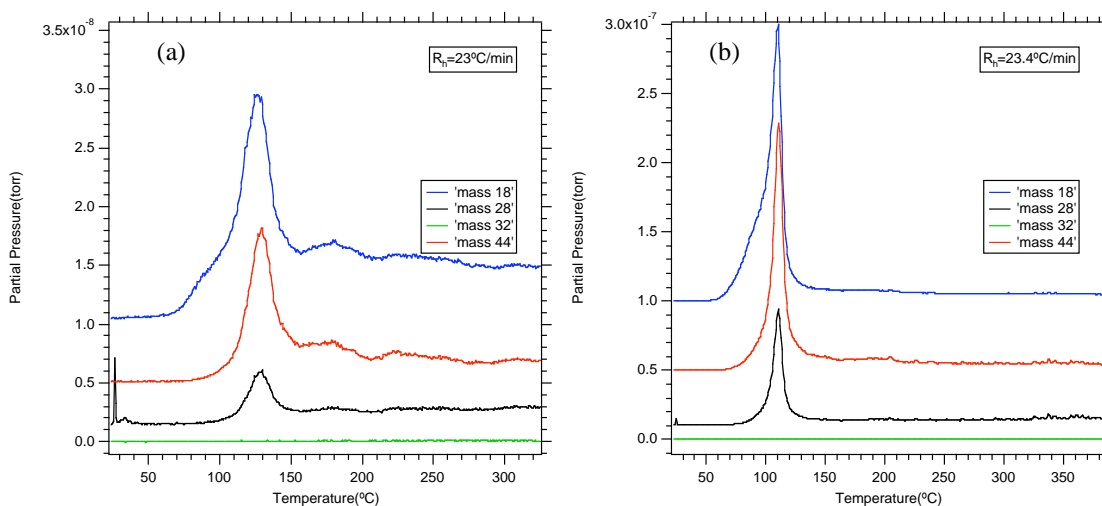


Figure 24: Partial Pressure vs. Temperature Curves for $R_h \sim 25\text{ }^\circ\text{C}/\text{min}$. (a) slow-stirred (b) ultrasonicated.

With a decrease in heating rate, it is shown in Figure 24 that the temperature at which the partial pressure peaks decreases. For the slow-stirred film, the temperature at the spike was 130 °C. For the ultrasonicated film, the pressure spike occurred at 110 °C. In the spectra for both heating rates, it is seen that the noise level decreases from slow-stirred to ultrasonicated and the measurement values of the partial pressures increase. It is suitable to note here that the intensity of the signal increases with the thickness of the sample. Another consistency seen from decreasing the heating rate is a downshift in peak of the partial pressure. The peak partial pressures from a heating rate of 50 to 25 °C/min between both films decreased by an average of 50%.

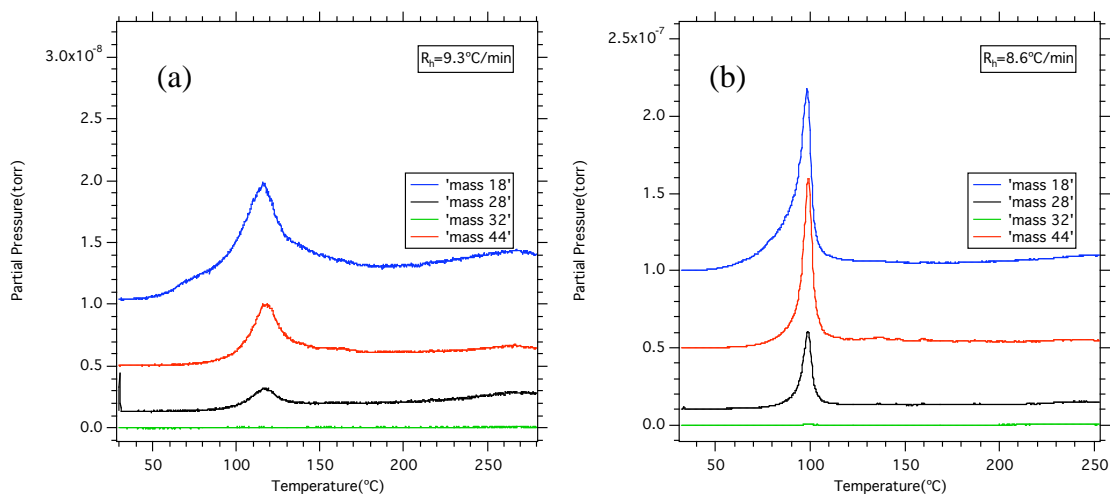
3. $R_h=10\text{ }^\circ\text{C}/\text{min}$ 

Figure 25: Partial Pressure vs. Temperature Curves for $R_h \sim 10\text{ }^\circ\text{C}/\text{min}$. (a) slow-stirred (b) ultrasonicated.

Here, with a heating rate of $10\text{ }^\circ\text{C}/\text{min}$, it is shown in Figure 25 that the peak temperature shifts even more to the left. For the slow-stirred film, the peak in partial pressure came at $116\text{ }^\circ\text{C}$. For the ultrasonicated film, the temperature at which the partial pressure peaked was at $98\text{ }^\circ\text{C}$. Additionally, consistent with the spectra for the other two heating rates, the thicker sample yielded a more intense signal being sent to the thermocouple.

E. Desorption Kinetics and Relative Coverages

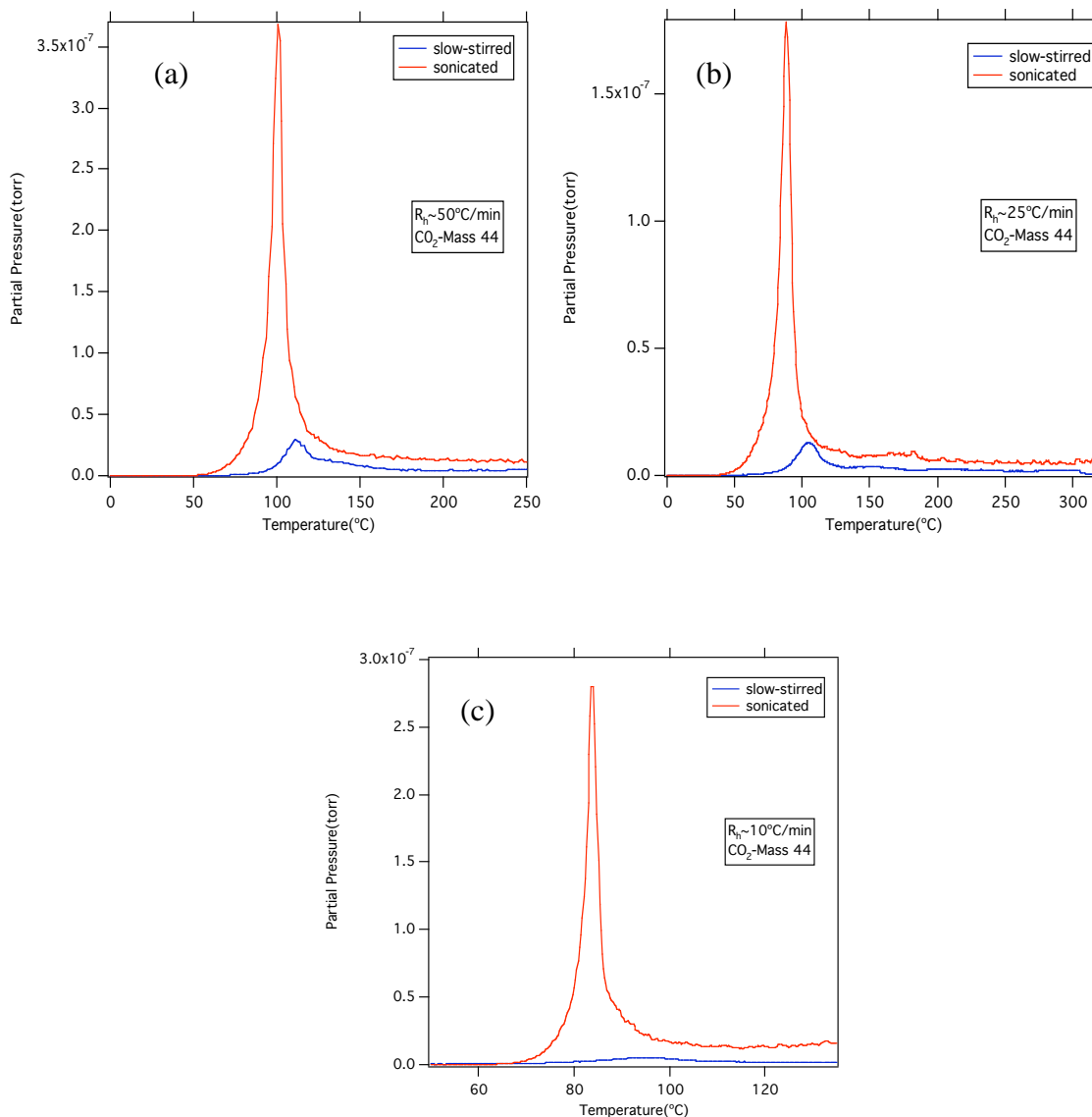


Figure 26: CO₂ Partial Pressure vs. Temperature Curves. (a) $R_h \sim 50$ (b) $R_h \sim 25$ (c) $R_h \sim 10$
Notice the shifts in T_m .

For each respective heating rate, the temperature peak shifts down with an increase in film thickness, as shown in Figure 26. Even though there is a downshift in the temperature, the order of kinetics is usually determined from temperature shifts in the partial pressure versus time curves for different coverages. The capability to test samples with different oxygen coverages was not possible in this experiment since all slow stirred and ultrasonicated graphene oxide films were all grown from two separate batches of graphene

oxide suspensions with fixed oxygen content. Therefore, the order of kinetics could not be determined directly. However, the relative coverages were obtained by plotting the partial pressure versus time and calculating the area under the curve. This was done for both the slow-stirred and ultrasonicated films with the three different heating rates.

Table 3: Area Under Partial Pressure vs. Time Curves

mass	Area Under the Curve(torr*sec) (with standard deviations)	
	Slow-stirred films	Ultrasonicated films
18	$2.27 \pm 0.34 \times 10^{-6}$	$7.96 \pm 0.16 \times 10^{-7}$
28	$5.39 \pm 0.76 \times 10^{-7}$	$2.66 \pm 0.47 \times 10^{-6}$
32	$1.41 \pm 0.39 \times 10^{-8}$	$2.73 \pm 0.15 \times 10^{-8}$
44	$1.01 \pm 0.11 \times 10^{-6}$	$5.80 \pm 0.87 \times 10^{-6}$

The average area under the pressure versus time curve for H₂O, CO, O₂, and CO₂ is shown in Table 3. The values for each mass were calculated for all heating rates, and then averaged to obtain the values in the table. From the data in the table, it is seen that the ratio of CO₂ to CO was 1.9 for the slow-stirred films and 2.2 for ultrasonicated films. In addition, the O₂ to CO₂ ratio was only 1.4% for the slow stirred films and 0.5% for the ultrasonicated films. Since CO₂ is not expected to exist as a component of the graphene oxide structure, it can be assumed the desorption has a recombinative nature. Spectra show that there are extremely small amounts of molecular oxygen, O₂, desorbing from the graphene oxide film. However, CO₂ is shown to be the second largest of peaks. Models show that oxygen exist on graphene oxide only as part of hydroxyl groups or as single oxygen atoms in the formation of monoxide(C=O) and epoxide groups(C-O-C). This means that in order to desorb as CO₂,

oxygen atoms travel and recombine with other oxygen atoms before coming off the surface. In addition, since hydrogen is only present in hydroxyl groups on the surface, this is true of hydrogen atoms. The recombination and CO_2/CO ratios explain the temperature shifts seen in Figure 27. The ratios show that there is a higher concentration of oxygen on the surface of the ultrasonicated films, which have a smaller platelet size. This means that, on average, an oxygen atom travels less distance, thus time, before recombining with another oxygen atom to desorb. Because of the linear relationship between time and temperature, the partial pressure peak comes at a lower temperature. The recombinative nature of the molecules desorbing off the surface is a characteristic of second order kinetics. Therefore, without being able to know exact coverages, it can be assumed that the order of kinetics, n , is ~ 2 .

F. Activation Energies

Before using the Arrhenius plotting method to find activation energies, the actual heating rates and peak temperatures of CO₂ were found and converted into the units of the Arrhenius equation.

Table 4: Data for Slow-Stirred Films

$T_m(K)$	$R_t(K/sec)$
408.196	0.97606
405.768	0.97537
402.317	0.484464
402.317	0.498842
392.221	0.198397

Actual value of heating rates and temperature maxima of CO₂ for slow-stirred films.

Table 5: Data for Ultrasonicated Films

$T_m(K)$	$R_t(K/sec)$
397.844	0.986629
383.019	0.49842
365.766	0.193783
383.658	0.492273

Actual value of heating rates and temperature maxima of CO₂ for ultrasonicated films.

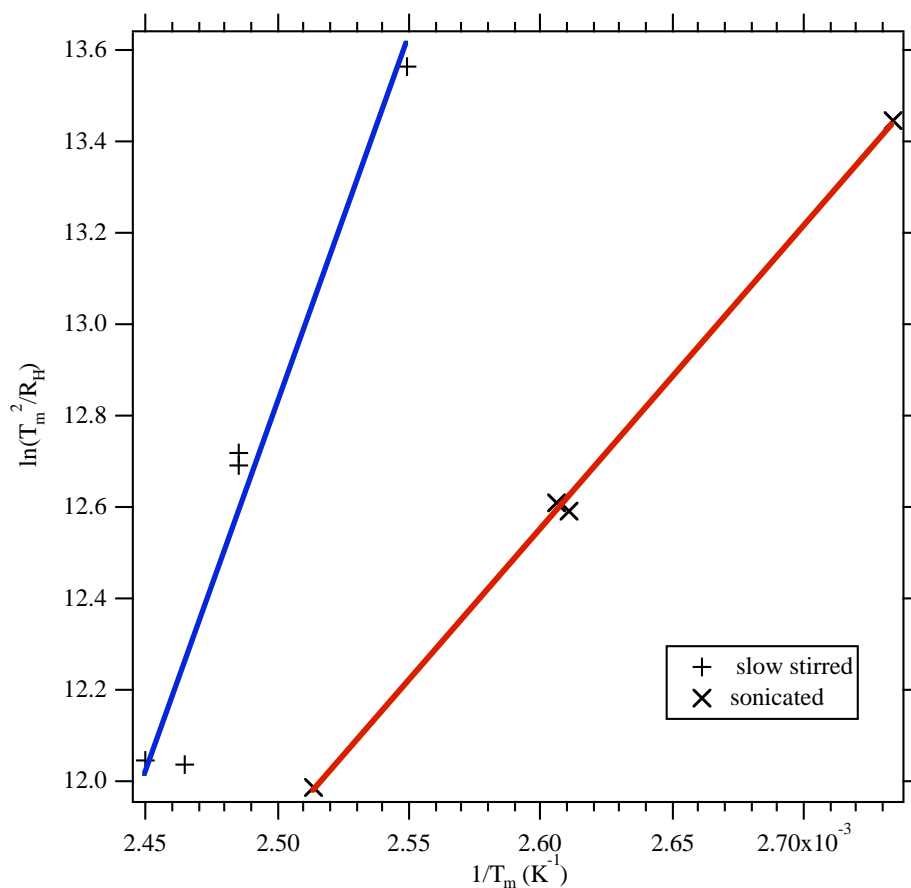


Figure 27: Activation energies of CO₂. Notice the different slopes for the slow-stirred and ultrasonicated films.

As previously mentioned, the slope of the $\ln(T_m/\beta)$ versus $1/T_m$ curve is equal to E_{des}/R . By obtaining the slope from a linear fit and multiplying by R , the gas constant, the activation energies of CO₂ for the slow-stirred and ultrasonicated films were calculated. For the slow-stirred films, an activation energy of 1.38eV was determined. For the ultrasonicated films, an activation energy of 0.57eV was determined. This large difference in the activation energies of the films prepared from the two different methods is somewhat unexpected. The most likely reason for the much smaller activation energy of the films grown from the

ultrasonicated graphene oxide is the much smaller platelet size. A full explanation of this effect will be given in the Discussion section.

To determine if isolated OH groups or O atoms are desorbing during the decomposition of the graphene oxide, TPD spectra for $m/z = 17$ and 16 were taken for samples prepared from slow-stirred and ultrasonicated graphene oxide platelets. Since the ionization of H_2O in the RGA also produces some OH (21%) and O (2%) and the ionization of CO_2 and CO also produce some O (9% and 2%, respectively), the measured spectra for $m/z = 17$ and 16 must be corrected for these cracking components. TPD spectra for $m/z = 17$, 16, and 15 taken from graphene oxide films grown from ultrasonicated and slow-stirred platelets are shown in Figure 28a and 28b, respectively. For the slow-stirred films (Figure 28b), there

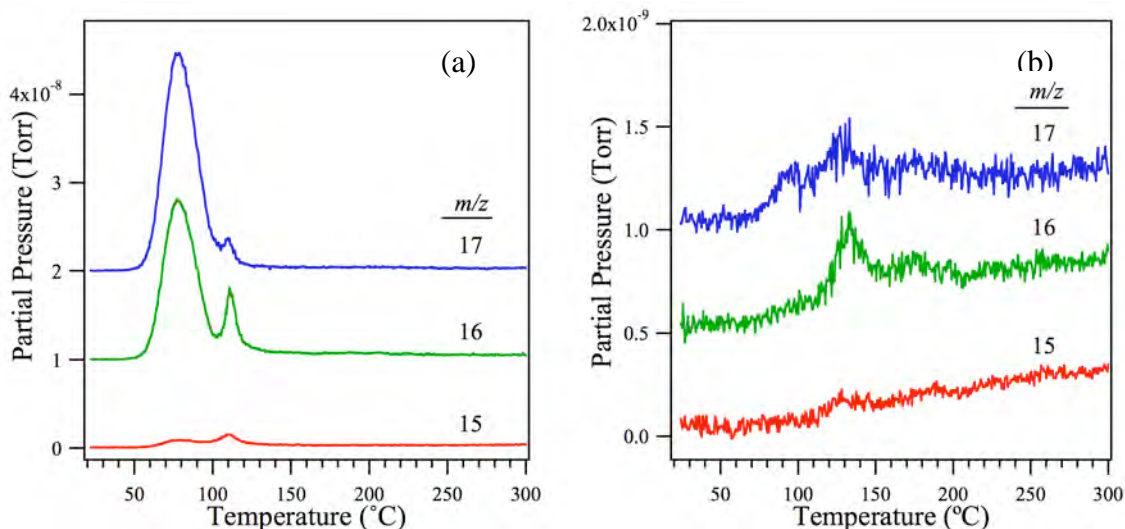


Figure 28: Ammonia Peaks. Partial Pressure vs. Temperature Spectra for masses 15, 16, and 17. (a) Ultrasonicated film. (b) Slow-stirred film.

is a small peak for $m/z = 16$ that is centered at 132 °C, which is probably due to methane (CH_4) desorption. However, for the ultrasonicated films, a large peak is observed for both

$m/z=17$ and 16 at $77\text{ }^\circ\text{C}$. Since there is virtually no desorption of O_2 ($m/z=32$) detected at this temperature, it is not likely that the detection of $m/z=16$ is from the direct desorption of O atoms. Since peaks for both $m/z=17$ and 16 are detected, the most likely source of these signals is from desorption of ammonia (NH_3) from the surface since its detection will result in peaks for $m/z=17$, 16 , and 15 due to the detection of NH_3 and its cracking components NH_2 and NH (80%, and 8%). The measured intensities of $m/z=16$ and 15 are 74% and 4%, which are reasonably close to the values expected for ammonia.

CHAPTER VI

DISCUSSION

It is important to understand the TPD spectra of graphene oxide in order to evaluate the use of this film in producing pristine graphene. The temperature ramping program proved to be consistent in providing constant heating rates so that Redhead method of TPD analysis could be followed. Furthermore, the pressure measurement program seemed to give relatively accurate measurements of the partial pressures. However, inconsistencies seen in the pressure measurement program are the dwell and settle time between readings. Since the dwell/settle is determined with a percentage in order to keep the signal to noise ratios identical, the amount of time it takes the SEM detector to find the right range and then measure is different upon each iteration.

The program measures the partial pressures of eight masses sequentially and then at the end of the last measurement outputs that data to an array with a time stamp of the time after the last measurement. Since there is a variation of the dwell time with each measurement, an exact time of each partial pressure measurement cannot be easily determined. Depending on the dwell/settle time of its respective iteration, it is possible that the time stamp given to a pressure measurement could be ~2sec off. This has minimal affect on the area under the curve for the partial pressure versus time curve because of the integration; however, this causes an inconsistency in the determination of the peak

temperature. By the partial pressure versus temperature graph being achieved by correlating the time data of each program, it is crucial that exact times of measurements are known.

The deviation of the time in the partial pressure measurement renders a peak temperature whose uncertainty deviates with the heating rate. For example, if the partial pressure measurement time stamp is 2 sec off, with a heating rate of 50 °C/min, or 0.83 °C/sec, there is uncertainty of 1.66 °C in the peak temperature. By affecting the peak temperature, this gives an inaccuracy in the calculation of the activation energy. In future experiments, this can be alleviated by setting the dwell/settle to absolute millisecond values and giving each partial pressure measurement its own array of time stamp. Another solution is structure one program that linearly ramps the temperature and simultaneously measures partial pressures along with the temperature at the time of measurement.

The implementation of the load lock system proved to be an efficient method of transferring graphene oxide sample into UHV without any damaging thermal treatment prior to TPD. Although successful in alleviating any substantial pre-TPD thermal behavior, it is impossible to verify good and consistent thermal contact with the sample each run. Each time the sample is mounted onto the stage, the thermocouple makes contact with the front of the sample, thus moving the thermocouple leads. This makes it impossible to dictate the position of the thermocouple on the sample, thus rendering inconsistent temperature measurements. In addition, because of the heat transfer between the thermocouple leads and the tungsten springs, there is a temperature difference between the point of contact and the rest of the graphene oxide film. The temperature at the contact point, T_{th} , turned out to be much cooler than the temperature of the sample, T_s . This temperature difference was measured by mounting a tantalum plate and heating the plate until it started to glow. The

plate was then further measured until the area around leads began to glow. This offset was measured and then taken accounted for in all of the spectra.

$$T_s = T_{th} + \frac{125}{450}(T_{th} - 25) \quad (6.1)$$

While troubleshooting the ramping program with a sample composed of another material, temperatures up to 450 °C were easily reached. It was assumed in the beginning of the graphene oxide test that the ramping program did not produce temperatures greater than 300 °C because the heating filament was bumped and off-centered during sample transfer. Midway through the testing, the chamber was vented and the heating filament was re-centered. In addition, the sample holder was redesigned with a tapered hole to allow e-beam heating of the samples. In all of the subsequent data, temperature shifts of up to 20 °C in T_m were observed for similar heating rates. With the inconsistency in the temperature readings with the new sample holder design, the activation energies could not be calculated accurately. Therefore, only the data taken before the chamber was vented was analyzed.

As previously discussed, the TPD spectra show only trace amounts of O₂ desorbing from the surface. Most of the oxygen that is desorbing from the graphene oxide is from H₂O, CO₂, and CO. The loss of carbon is detrimental since the ultimate goal is to be able to deoxidize graphene oxide down to pristine graphene. Since carbon is the backbone of graphene, a loss of carbon during chemical reduction results in defects within the layer of graphene. These defects will make it hard to recover the electrical properties of pristine graphene.

The difference in activation energies from the ultrasonicated films to the slow-stirred are justified by the recombinative nature of desorption and the platelet size of the film. If most of the desorption is occurring at the edges of the platelets, the larger platelet size of the

slow stirred films gives the molecules more area to travel before desorbing. Conversely, the ultrasonicated films are considerably smaller, thus requiring less diffusion before desorption.

In addition, from the spectra of the curves of masses 15, 16, and 17 (Figure 28), ammonia is detected in the ultrasonicated films and not in the slow-stirred films. This is also assumed to be a result of the smaller platelet sizes of the ultrasonicated films. Since there are ten times more edge sites for the ultrasonicated films than for the slow-stirred films, it is speculated that the edge sites are more reactive. Because of this, there are more sites on the ultrasonicated films that could possibly pick up any ammonia that was present during the synthesis or transportation of the films.

CHAPTER VII

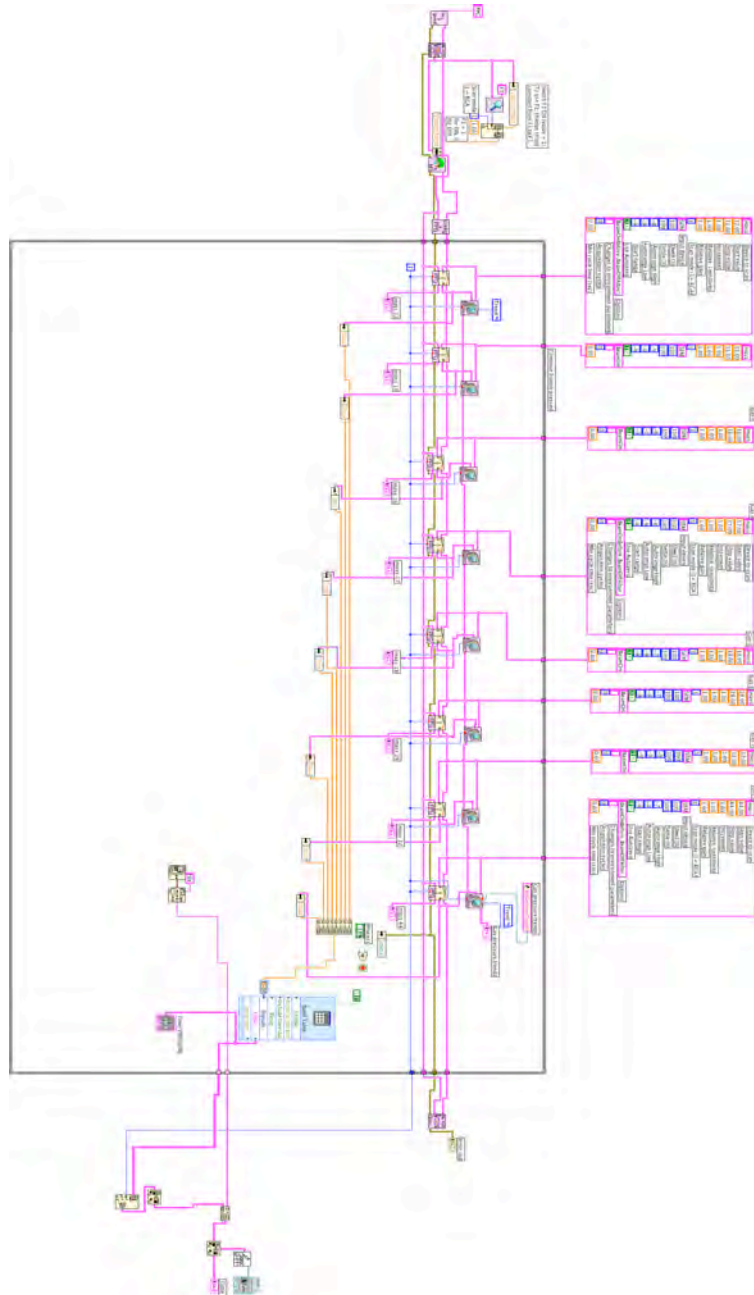
CONCLUSION

Two programs were designed and written in order to produce consistent linear heating ramps and obtain partial pressure measurements for TPD analysis. A linear temperature ramp is essential for finding activation energies and the kinetics of desorption because a constant heating rate makes it possible to utilize Redhead's method of analyzing TPD data. Previous studies show that desorption of species on graphene oxide takes place at relatively low temperatures. The unique TPD system at Texas State University-San Marcos made it possible to transfer graphene oxide samples into UHV conditions with no substantial thermal damages and accurately measure the partial pressures and temperature peaks of desorbing molecules.

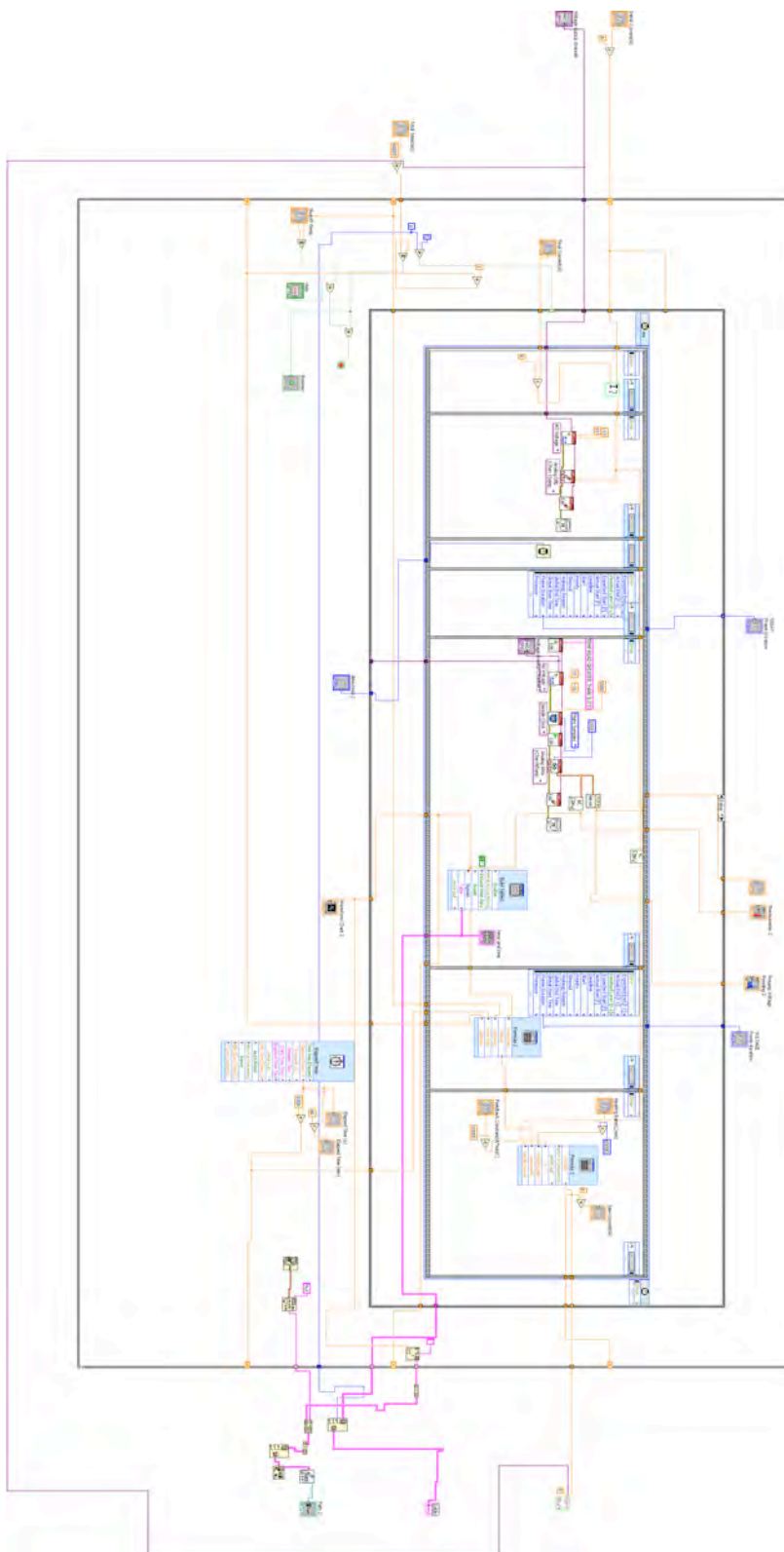
Activation energies for CO₂ were found for graphene oxide films exfoliated from an aqueous solution of graphite oxide by slow-stirring and ultrasonication. For slow-stirred films the activation energy was 1.38eV and for ultrasonicated films the activation energy was 0.58eV. Results show that the activation energy of molecules is highly dependent upon the concentration of the molecule and the platelet sizes of the films. In addition, TPD spectra show the importance of accurately measuring the temperature. If temperature measurements are not consistent, the activation energies of desorbing molecules cannot be accurately calculated.

APPENDIX A
BLOCK DIAGRAMS

Partial Pressure Measurement Program:



Temperature Ramp Program:



APPENDIX B
CRACKING PATTERNS

	Name	Formula	peak 1		peak 2		peak 3		rel sens
			m/z	%	m/z	%	m/z	%	
1	acetone	C ₃ H ₆ O	43	100	58	33	15	20	3.6
2	air		28	100	32	27	14	6	1.0
3	ammonia	NH ₃	17	100	16	80	15	8	1.3
4	argon	Ar	40	100	20	16	36	0.3	1.2
5	benzene	C ₆ H ₆	78	100	77	19	52	16	5.9
6	boron trichloride	BCl ₃	81	100	83	65	35	29	1.0
7	carbon dioxide	CO ₂	44	100	16	9	28	8	1.4
8	carbon monoxide	CO	28	100	12	5	16	2	1.05
9	carbon tetrafluoride	CF ₄	69	100	50	12	19	7	1.0
10	diborane	B ₂ H ₆	26	100	27	97	24	90	1.0
11	ethane	C ₂ H ₆	28	100	27	33	30	26	2.6
12	ethanol	C ₂ H ₅ OH	31	100	45	51	29	30	3.6
13	Fomblin oil		69	100	20	28	16	16	1.0
14	Freon 12	CCl ₂ F ₂	85	100	87	32	50	16	2.7
15	helium	He	4	100					0.14
16	hydrogen	H ₂	2	100	1	2			0.44

Cracking Patterns (continued)

17	hydrogen chloride	HCl	36	100	38	32	35	17	1.6
18	hydrogen sulphide	H ₂ S	34	100	32	44	33	42	2.2
19	isopropyl alcohol	C ₃ H ₇ OH	45	100	43	14	27	9	1.0
20	krypton	Kr	84	100	86	31	82	21	1.7
21	methane	CH ₄	16	100	15	85	14	16	1.6
22	methanol	CH ₃ OH	31	100	32	67	29	65	1.8
23	neon	Ne	20	100	22	10	21	0.3	0.23
24	nitrogen	N ₂	28	100	14	5	29	1	1.0
25	oxygen	O ₂	32	100	16	9			0.86
26	phosphine	PH ₃	34	100	33	33	31	32	2.6
27	pump oil		57	100	55	73	43	73	1.0
28	silane	SiH ₄	30	100	31	78	29	29	1.0
29	silicon tetrafluoride	SiF ₄	85	100	86	5	28	4	1.0
30	sulphur dioxide	SO ₂	64	100	48	50	32	10	2.1
31	water	H ₂ O	18	100	17	21	16	2	0.9
32	xenon	Xe	132	100	129	98	131	79	3.0

REFERENCES

1. A. Geim and K. Novoselov, *The Rise of Graphene*, Nature **6**, 183 (2007).
2. D. Yang, A. Velamakannie, G. Bozoklu, A. Park, M. Stoller, R. D. Piner, S. Stankovich, I. Jung, D. A. Field, C. A. Ventrice, and R. S. Ruoff, *Chemical Analysis of Graphene Oxide Films After Heat and Chemical Treatments by X-ray Photoelectron and Micro-Raman Spectroscopy*, Carbon **47**, 145 (2009).
3. *Omega Complete Temperature Measurement Handbook and Encyclopedia: Type K Thermocouple Temperature Coefficients*, Vol. 28 (Omega Engineering, Stamford, Connecticut, 1992).
4. P.A. Redhead, *Thermal Desorption of Gases*, Vacuum **12**, 203 (1962).
5. J.W. Niemantsverdriet, *Spectroscopy in catalysis: An Introduction*, 2nd ed. (Wiley-VCH, 2000).
6. Van Bramer, S.E., *An Introduction to Mass Spectrometry*, Manual of Mass Spectrometry.
7. T. Russell (private communication, 2008).
8. Z. Cambaz, G. Yushin, S. Osswald, V. Mochalin, and Y. Gogotsi, *Noncatalytic Synthesis of Carbon Nanotubes, Graphene and Graphite on SiC*, Carbon **46**, 841 (2008).
9. G. Yuan, W. Zhang, Y. Yang, Y. Tang, and I. Bello, *Graphene Sheets via Microwave Chemical Vapor Deposition*, Carbon **467**, 361 (2009).
10. D. Dikin, S. Stankovich, E. Zimney, R. Piner, G. Dommett, G. Evmenenko, S. Nguyen, and R. Ruoff, *Preparation and Characterization of Graphene Oxide Paper*, Nature **448**, 457 (2007).
11. K. Kudin, B. Ozbas, H. Schniepp, R. Prud'homme, I. Aksay, and R. Car, *Raman Spectra of Graphite Oxide and Functionalized Graphene Sheets*, Nanoletters **8**, 36 (2008).
12. S. Stankovich, D. Dikin, G. Dommett, K. Kohlhaas, E. Zimney, E. Stach, R. Piner, S. Nguyen, and R. Ruoff, *Graphene-based Composite Materials*, Nature **442**, 282 (2006).
13. A. Cabrera, *Kinetic Parameters Obtained from Integration of Single Peak Thermal Desorption Spectra*, Journal of Chemical Physics **93**, 2854 (1990).

14. E. Kautto, J. Kuhalainen, and M. Manninen, *Analysing Methods for Thermal Desorption Spectra*, *Physica Scripta* **55**, 628 (1997).
15. Boltzmann Statistics, <http://www.physics.ubc.ca/~birger/boltzmann/node1.html>.
16. F. Reif, *Fundamentals of Statistical and Thermal Physics* (McGraw Hill, Boston, MA., 1965), pp.331-397.
17. Quadrupole Mass Spectrometry, <http://www.files.chem.vt.edu/chem-ed/ms/quadrupo.html>.
18. Szabó et al., *Chem. Mater.* **18**, 2740 (2006).
19. D. Field, M.S. Thesis, Texas State University-San Marcos, 2008.
20. Omega.com, <http://www.omega.com/>
21. IGOR Pro, *Getting Started* (WaveMetrics, Inc., Lake Oswego, OR, 2007).
22. LabVIEW, *LabVIEW Fundamentals* (National Instruments, Austin, TX, 1999)

VITA

Nicholas J. Clark was born on July 23, 1985 to Jeffie and LaQuita Clark in Fort Worth, Texas. He has an older sister, April, and a younger brother, Marcus. Nick attended Everman Joe C. Bean high school where he was a standout athlete and student.

After graduating, Nick continued his academic and football career at the Navel Academy Preparatory School. In Spring 2004 he enrolled at Texas State University-San Marcos. While playing football for the Bobcats, he started as a true freshman and held his starting role for four years, winning a Southland Conference Championship along the way. He excelled on the field and off the field by being chosen for the NCAA's highest student-athlete award, the Draddy Award. He was awarded a Bachelor of Science in Mathematics before his fourth year of football in August 2007.

In Fall 2007 Nick began his graduate research in the Department of Physics at Texas State. During his tenure in graduate school he developed an automated measurement system in order to perform temperature programmed desorption studies on the surface of materials in ultra high vacuum.

In the fall of 2010, Nick plans to further his education and earn a PhD in a field related to Physics. Until then, he will play and compose music as a full-time musician.

Permanent Address: 1408 Glasgow Rd.

Fort Worth, TX 76134

This thesis was typed by Nicholas J. Clark.